PREPRINT

Experimental Evidence for Linear Metal-Azide Bonds. The Binary Group 5 Azides $Nb(N_3)_5$, $Ta(N_3)_5$, $[Nb(N_3)_6]^-$ and $[Ta(N_3)_6]^-$, and 1:1 Adducts of $Nb(N_3)_5$ and $Ta(N_3)_5$ with CH_3CN [**]

Ralf Haiges[*], Jerry A. Boatz, Thorsten Schroer, Muhammed Yousufuddin, and Karl O. Christe[*]

Whereas numerous binary transition metal azido-complexes have been reported,[1-3] no binary Group 5 azides are known. Only a limited number of partially azide-substituted compounds of vanadium, niobium and tantalum have previously been reported.[4-21]

In this paper, we wish to communicate the synthesis and characterization of $Nb(N_3)_5$, $Ta(N_3)_5$ and their 1:1 adducts with CH_3CN, and of the anions $[Nb(N_3)_6]^-$ and $[Ta(N_3)_6]^-$. We also report the crystal structures of $Nb(N_3)_5 \cdot CH_3CN$ and $[PPh_4][Nb(N_3)_6]$ and the first experimental evidence for the existence of azido compounds with linear metal-N-N bonds.

The reactions of NbF_5 or TaF_5 with excess $(CH_3)_3SiN_3$ in SO_2 solution at -20 °C result in complete fluoride-azide exchange and yield clear solutions of $Nb(N_3)_5$ or $Ta(N_3)_5$, respectively, [Eq. (1) (M = Nb, Ta)].

$$MF_5 + 5\,(CH_3)_3SiN_3 \longrightarrow M(N_3)_5 + 5\,(CH_3)_3SiF \qquad (1)$$

Pumping off the volatile compounds, SO_2, $(CH_3)_3SiF$ and excess $(CH_3)_3SiN_3$), at -20 °C

---

[*] Dr. R. Haiges, Dr. T. Schroer, M. Yousufuddin, Prof. Dr. K. O. Christe
Loker Research Institute and Department of Chemistry
University of Southern California
Los Angeles, CA 90089-1661 (USA)
Fax: (+1) 213-740-6679
E-mail: haiges@usc.edu, kchriste@usc.edu
Dr. J. A. Boatz
Space and Missile Propulsion Division
Air Force Research Laboratory (AFRL/PRSP)
10 East Saturn Boulevard, Bldg 8451
Edwards Air Force Base, CA 93524 (USA)

[**] This work was funded by the Air Force Office of Scientific Research and the National Science Foundation. We thank Prof. Dr. G. A. Olah, and Dr. M. Berman, for their steady support, and Prof. Dr. R. Bau and Drs. S. Schneider and R. Wagner for their help and stimulating discussions.

Report Documentation Page

Form Approved
OMB No. 0704-0188

1. REPORT DATE	2. REPORT TYPE	3. DATES COVERED
27 APR 2005	**Journal Article**	**00-04-2005 to 00-04-2005**

4. TITLE AND SUBTITLE	5a. CONTRACT NUMBER
Experimental Evidence for Linear Metal-Azide Bonds. The Binary Group 5 Azides Nb(N3)5, Ta(N3)5, [Nb(N3)6]- and [Ta(N3)6]-, and 1:1 Adducts of Nb(N3)5 and Ta(N3)5 with CH3CN (PREPRINT)	5b. GRANT NUMBER
	5c. PROGRAM ELEMENT NUMBER

6. AUTHOR(S)	5d. PROJECT NUMBER
Ralf Haiges; Jerry Boatz; Thorsten Schroer; Muhammed Yousufuddin; Karl Christe	**2303**
	5e. TASK NUMBER **0423**
	5f. WORK UNIT NUMBER

7. PERFORMING ORGANIZATION NAME(S) AND ADDRESS(ES)	8. PERFORMING ORGANIZATION REPORT NUMBER
Air Force Research Laboratory (AFMC),AFRL/PRSP,10 E. Saturn Blvd.,Edwards AFB,CA,93524-7680	**AFRL-PR-ED-JA-2005-162**

9. SPONSORING/MONITORING AGENCY NAME(S) AND ADDRESS(ES)	10. SPONSOR/MONITOR'S ACRONYM(S)
Air Force Research Laboratory (AFMC), AFRL/PRS, 5 Pollux Drive, Edwards AFB, CA, 93524-7048	**XC**
	11. SPONSOR/MONITOR'S REPORT NUMBER(S) **AFRL-PR-ED-JA-2005-162**

12. DISTRIBUTION/AVAILABILITY STATEMENT
Approved for public release; distribution unlimited

13. SUPPLEMENTARY NOTES
Submitted to the Journal: Angewandte Chemie

14. ABSTRACT

Whereas numerous binary transition metal azido-complexes have been reported,[1-3] no binary Group 5 azides are known. Only a limited number of partially azide-substituted com-pounds of vanadium, niobium and tantalum have previously been reported.[4-21] In this paper, we wish to communicate the synthesis and characterization of Nb(N3)5, Ta(N3)5 and their 1:1 adducts with CH3CN, and of the anions [Nb(N3)6]- and [Ta(N3)6]-. We also report the crystal structures of Nb(N3)5·CH3CN and [PPh4][Nb(N3)6] and the first experimental evidence for the existence of azido compounds with linear metal-N-N bonds.

15. SUBJECT TERMS

16. SECURITY CLASSIFICATION OF:			17. LIMITATION OF ABSTRACT	18. NUMBER OF PAGES	19a. NAME OF RESPONSIBLE PERSON
a. REPORT	b. ABSTRACT	c. THIS PAGE			
unclassified	**unclassified**	**unclassified**		**38**	

produces the pure, yellow, solid, room-temperature stable pentaazides in quantitative yield. As expected for covalently bonded polyazides,[22] they are shock sensitive and can explode violently when touched with a metal spatula or by heating in the flame of a Bunsen burner. Their identity was established by the observed mass-balances, vibrational spectroscopy and their conversions with N_3^- into hexaazido-metalates and with CH_3CN into 1:1 acetonitrile donor-acceptor adducts, as shown by the crystal structures of $[P(C_6H_5)_4]^+[Nb(N_3)_6]^-$ and $Nb(N_3)_5 \cdot CH_3CN$. The reaction of VF_5 with $(CH_3)_3SiN_3$ was also briefly studied, and fluoride/azide exchange was observed. However, because VF_5 is a stronger oxidizer than NbF_5 and TaF_5 and the azide ion is a strong reducing agent, the product was poorly defined (black solid, Ra 2094 [4.5], 2052 [2.7], 483 [10], 434 [8.0], 383 [5.7]), and the reaction was not further pursued.

The observed infrared and Raman spectra of $Nb(N_3)_5$ and $Ta(N_3)_5$ are shown in Figures 1 and 2, respectively, and the observed frequencies and intensities are listed in the Experimental Section. They were assigned (see Tables S1 and S2 of the Supplementary Material) by comparison with those calculated at the B3LYP[23] and MP2[24] levels of theory using SBKJ-(d) basis sets.[25] The agreement between observed and calculated spectra is satisfactory and supports trigonal-bipyramidal structures (Figure 3) for $Nb(N_3)_5$ and $Ta(N_3)_5$. The internal modes of the azido ligands are split into clusters of five due to in-phase and out-of-phase coupling of the individual motions. There are always one in-phase and four out-of-phase vibrations, with the in-phase one readily identifiable from its higher Raman intensity. The MN_5 skeletal modes can be derived from D_{3h} symmetry in which the double degeneracy of the E modes is lifted due to the presence of the azido ligands which lowers the overall symmetry to C_s and is likely to produce some distortion from D_{3h}.

Whereas trigonal-bipyramidal arrangements of the azido ligands have previously also been found for $[Fe(N_3)_5]^{2-}$,[26] $Sb(N_3)_5$and $As(N_3)_5$,[27,28] the details of these structures are very different. In $[Fe(N_3)_5]^{2-}$, $As(N_3)_5$ and $Sb(N_3)_5$, all five M-N-N bonds are strongly bent, and the two axial M-N bonds are significantly longer than the equatorial ones, as expected from VSEPR arguments.[29] In contrast, the axial M-N-N bonds in $Nb(N_3)_5$ and $Ta(N_3)_5$ are almost linear, while the equatorial ones have angles of about 137 °. Furthermore, all five M-N bonds and the internal N-N distances of the five azido ligands are essentially the same.

Linear M-N-N bonds had previously been predicted also for the tetraazides of d^0 Ti(+IV), Zr(+IV), and Hf(+IV)[30] and for d^6 Fe(+II),[1] but the hexazido dianion of d^0 Ti(+IV) was shown to possess strongly bent Ti-N-N bonds.[1] These findings show that the linearity of the M-N-N bonds cannot be caused by either a trigonal-bipyramidal structure, multiple M-N bonds, or a d^0 electronic configuration *per se*.

A plausible explanation for the linearity of these M-N-N bonds has recently been proposed.[1] It is based on the recognition that, in a covalent azide, the two free valence electron pairs on the N_α atom can participate in the donation of electron density to the central metal atom. Therefore, depending on the availability of suitable empty orbitals on the metal center, the N_α atom can function as either a mono-, bi-, or tri-dative donor, thereby influencing the M-N-N bond angle (Figure 4). In the monodative binding mode, the M-N-N bong angle is close to tetrahedral, (~ 107 ° or somewhat larger). This is the case for main group elements which involve mainly the single-lobe *s* and *p* orbitals of the central atom. Typical examples are: $[C(N_3)_3]^+$ (108 °),[31] $[B(N_3)_4]^-$ (117.6 °),[32] $[As(N_3)_6]^-$ (115.6 °),[33] and $[Te(N_3)_6]^{2-}$ (109.3 and 121.2 °).[34] In transition metals, the presence of *d* orbitals offers additional lobes for overlap and, as a result, the N_α atom can act as either a monodative, bidative, or tridative donor with M-N-N bond angles

ranging from 118 ° in monodative $Hg_2(N_3)_2$[35] to about 180 ° in tridative $Ti(N_3)_4$, $Zr(N_3)_4$, $Hf(N_3)_4$,[30] $Fe(N_3)_2$,[1] $V(N_3)_5$, $Nb(N_3)_5$, $Ta(N_3)_5$, and $CH_3CN{\cdot}Nb(N_3)_5$. A typical M-N-N bond angle range for a bidative donor mode appears to be about 135 °, as found for $W(N_3)_6$[2] and the equatorial ligands in $Nb(N_3)_5$ or $Ta(N_3)_5$. Based on the calculated bond angles, the axial azido ligands in $Nb(N_3)_5$ and $Ta(N_3)_5$ would involve tridative donor bonds, while the equatorial ones would constitute bidative ones. A preliminary analysis of the presently known azido compounds with linear M-N-N bonds indicates that all of them obey the following condition [Eq. (2)]:

(number of monodative ligands x 1) + (number of bidative ligands x 2) + (number of tridative ligands x 3) + (number of *d* electrons of the cationic center) = 12 (2)

The lowest-energy vacant orbitals in these transition metal centers are the s^2 electrons of the valence shell and the d^{10} electrons from the next lower shell. The "magic number 12" in Eq. 2 can be rationalized by a tendency of the metal centers to obtain an energetically favorable filled s^2d^{10} electron shell. This objective is achieved by involving as many free valence electron pairs of the α-nitrogen atoms of azido ligands in the bonding as needed for reaching the "magic number 12". Thus, Eq. 2 provides a simple way to predict whether in transition metal complexes an azide ligand will be mono-, bi-, or tri-dative. For example, in $Nb(N_3)_5$ and $Ta(N_3)_5$ we have d^0 metal centers, three bidative and two tridative ligands, i.e., 0 + 3x2 + 2x3 = 12; in $Fe(N_3)_2$ we have d^6 Fe(II) and two tridative azido groups, i.e., 6 + 2x3 = 12; in $Ti(N_3)_4$ we have d^0 Ti(IV) and four tridative ligands, i.e., 0 + 4x3 = 12. Although there have been two recent molecular orbital studies on the closely related tridentate $Zr(BH_4)_4$ adduct[1,36] and on tridative $Ti(N_3)_4$[30], neither one recognized the simple correlation given by Eq. 2.

Some comment is required about the terminology of "multidative" bonds proposed above. We have carefully considered the uses of either "mono-, bi-, or tri-dentate" or "single,

double, or triple" bonds in place of "mono-, bi-, or tri-dative" bonds, but were dissatisfied with either choice. The term "multidentate" is defined as bonding through multiple atoms, and "multiple bonds" imply bond orders which are significantly higher than one. Neither situation correctly describes the bonding shown in these azides. In the linear metal azides, the metal-N_α bond clearly does not possess triple bond character, although three α-nitrogen electron pairs participate in the bonding. The definition of what constitutes a chemical bond and, particularly, what constitutes a multiple bond presents a very general problem, and the lack of clear definitions, combined with the zeal of publicity-hungry chemists for novelty, has led to widespread and abusive claims.

By using CH_3CN instead of SO_2 as solvent for the reactions of NbF_5 and TaF_5 with excess $(CH_3)_3SiN_3$, yellow solutions of $CH_3CN{\cdot}Nb(N_3)_5$ and $CH_3CN{\cdot}Ta(N_3)_5$, respectively, were obtained [Eq. (3) (M = Nb, Ta)].

$$MF_5 + 5\,(CH_3)_3SiN_3 \longrightarrow CH_3CN{\cdot}M(N_3)_5 + 5\,(CH_3)_3SiF \qquad (3)$$

Removal of the volatile compounds (CH_3CN, $(CH_3)_3SiF$ and excess $(CH_3)_3SiN_3$) at -20 °C results in the isolation of the acetonitrile-adducts of the pentaazides. Although still dangerous and explosive, both acetonitrile-adducts are less shock-sensitive than the corresponding donor-free pentaazides.

Both acetonitrile-adducts were isolated as yellow solids and were characterized by vibrational spectroscopy, their conversion with N_3^- into the hexaazido-metalates and, in the case of $CH_3CN{\cdot}Nb(N_3)_5$, by its crystal structure.[37] The observed Raman spectra of $CH_3CN{\cdot}Nb(N_3)_5$ and $CH_3CN{\cdot}Ta(N_3)_5$ are shown in Figures 5 and 6, respectively, and their frequencies and intensities are given in the Experimental Section. A comparison with the calculated spectra is

given in Tables S3 and S4 of the Supplementary Material, and the given assignments are in accord with those previously reported[38,39] for the related $CH_3CN{\cdot}SbF_5$ adduct.

$CH_3CN{\cdot}Nb(N_3)_5$ crystallizes in the monoclinic space group *P*2(1)/*c*. The X-ray structure analysis[37] (Figure 7) reveals the presence of isolated $CH_3CN{\cdot}Nb(N_3)_5$ units. The closest Nb···N and N···N contacts between neighboring molecules are 3.98 Å and 3.04 Å, respectively.

The molecule consists of a pseudo-octahedral NbN_6 skeleton with CH_3CN and one azido group in the axial positions. The equatorial positions are occupied by the remaining 4 azido groups which, interestingly, are all bent away from the axial azido ligand. The axial Nb-N3 distance is about 0.09 Å shorter than the four equatorial ones. The most interesting feature, however, is the fact that the axial azido group exhibits a large Nb-N-NN bond angle of 168.8º, compared to an average angle of 137.8º for the four equatorial ligands, and suggests the presence of a tridative azido ligand. The minor deviation of the observed axial Nb-N-N angle from the ideal 180º is attributed to solid state effects, because our theoretical calculations for the free gaseous molecule at the B3LYP and MP2 levels of theory with an SBKJ+(d) basis set resulted in Nb-N-N angles of 179.6º and 179.2º, respectively. Again, the rule of 12 [0 *d* electrons, 1 mono-dative ligand (CH_3CN), four bidative ligands (equatorial azides) and one tridative ligand (axial azide), corresponding to 0 + 1x1 + 4x2 +1x3 = 12] is fulfilled.

The average $Nb\text{-}N_{azide}$ distance of 1.997 Å in $CH_3CN{\cdot}Nb(N_3)_5$ is significantly shorter than those of 2.081 Å and 2.105 Å found for the terminal azides of two isomers of $[Cp^*NbCl(N_3)(\mu\text{-}N_3)]_2(\mu\text{-}O)$[16] and 2.27 Å found for the cluster $[Nb_6Br_{12}(N_3)_6]^{4-}$,[18] but slightly longer than that of 1.92 Å found in $[NbCl_5(N_3)]^-$ [19] and is attributed to varying degrees of ionicity of the azide ligands in these compounds.

The reactions of the pentaazides with ionic azides, such as $[P(C_6H_5)_4]^+N_3^-$, in CH_3CN solution produce the corresponding $[Nb(N_3)_6]^-$ and $[Ta(N_3)_6]^-$ salts, respectively, [Eq. (4) (M = Nb, Ta].

$$M(N_3)_5 + [P(C_6H_5)_4]N_3 \longrightarrow [P(C_6H_5)_4][M(N_3)_6] \quad (4)$$

The hexaazido metalates of niobium and tantalum were isolated as yellow-orange solids and are stable at room temperature. The compounds were characterized by the observed material balances, vibrational spectroscopy, and in the case of $[P(C_6H_5)_4][Nb(N_3)_6]$ by its crystal structure.[40] The observed vibrational spectra of $[P(C_6H_5)_4][Nb(N_3)_6]$ and $[P(C_6H_5)_4][Ta(N_3)_6]$ are shown in Figure 8 and 9, respectively, and their frequencies and intensities are given in Table 1 and the Experimental Section, respectively. The free gaseous $Nb(N_3)_6^-$ anion is predicted to have perfect S_6 ($\equiv C_{3i}$) symmetry, which is quite rare,[41] and, therefore, a complete vibrational analysis was carried out (Table 1). $Ta(N_3)_6^-$ is slightly distorted from S_6 to C_1 symmetry, but its structure is almost identical to that of $Nb(N_3)_6^-$, and the splittings of its degenerate modes are extremely small (Table S5 of the Supplementary Material).

Because of the presence of a large counter-ion which serves as an inert spacer and suppresses detonation propagation, these salts are much less shock sensitive than neat $Nb(N_3)_5$ and $Ta(N_3)_5$, and are thermally surprisingly stable. Single crystals of $[P(C_6H_5)_4][Nb(N_3)_6]$ were obtained by re-crystallization from CH_3CN. The salt crystallizes in the rare orthorhombic space group *P*2(1)2(1)2. The X-ray structure analysis[40] of $[P(C_6H_5)_4][Nb(N_3)_6]$ (Figure 10) reveals no significant cation-anion and anion-anion interactions. The closest Nb···N and N···N contacts between neighboring anions are 4.20 Å and 3.15 Å, respectively. The structure of the $[Nb(N_3)_6]^-$ anion in the solid is only slightly distorted from the perfect S_6 symmetry, predicted by our theoretical calculations for the free gaseous anion, and is similar to those of $[As(N_3)_6]^-$[28],

$[Sb(N_3)_6]^-$,[27] $[Si(N_3)_6]^-$[42] $[Ge(N_3)_6]^-$[43] and $[Ti(N_3)_6]^{2-}$,[1] and contrary to that of $[Te(N_3)_6]^-$[34] which contains a sterically active free valence electron pair on its central atom. The average Nb-N distance of 2.027 Å in $[Nb(N_3)_6]^-$ is larger than that of 1.997 Å found for $CH_3CN{\cdot}Nb(N_3)_5$, as expected from the formal negative charge in the former which increases the ionic character of the azide ligands. The average Nb-N-N bond angle in $[Nb(N_3)_6]^-$ amounts to 143 °, indicative of six bidative azido ligands. This in accord with the rule of 12, as $[Nb(N_3)_6]^-$ possesses zero monodative and tridative ligands and Nb(+V) is a d^0 center. The relatively large variation in the Nb-N-N bond angles, which range from 131.7 to156.2°, is attributed to intramolecular repulsion effects among the ligands.

Experimental Section

Caution! *Covalent azides are potentially hazardous and can decompose explosively under various conditions! The polyazides of this work are extremely shock-sensitive and can explode violently upon the slightest provocation. They should be handled only on a scale of less than 1 mmol. Because of the high energy content and high detonation velocities of these azides, their explosions are particularly violent and can cause, even on a one mmol scale, significant damage. The use of appropriate safety precautions (safety shields, face shields, leather gloves, protective clothing, such as heavy leather welding suits and ear plugs) is mandatory. Teflon containers should be used, whenever possible, to avoid hazardous shrapnel formation. The manipulation of these materials is facilitated by handling them, whenever possible, in solution to avoid detonation propagation, the use of large inert counter-ions as spacers, and anion formation which increases the partial negative charges on the terminal N_γ atoms and thereby*

reduces the N_β-N_γ triple bond character. ***Ignoring safety precautions can lead to serious injuries!***

Materials and Apparatus: All reactions were carried out in Teflon-FEP ampules that were closed by stainless steel valves. Volatile materials were handled in a Pyrex glass or stainless steel/Teflon-FEP vacuum line.[44] All reaction vessels were passivated with ClF_3 prior to use. Nonvolatile materials were handled in the dry argon atmosphere of a glove box.

Raman spectra were recorded directly in the Teflon reactors in the range 4000–80 cm^{-1} on a Bruker Equinox 55 FT-RA spectrophotometer, using a Nd-YAG laser at 1064 nm with power levels less than 50 mW(!). Infrared spectra were recorded in the range 4000-400 cm^{-1} on a Midac, M Series, FT-IR spectrometer using KBr pellets. The pellets were prepared inside the glove box using an Econo mini-press (Barnes Engineering Co.) and transferred in a closed container to the spectrometer before placing them quickly into the sample compartment which was purged with dry nitrogen to minimize exposure to atmospheric moisture and potential hydrolysis of the sample.

The starting materials NbF_5, TaF_5 (both Ozark Mahoning) and $[P(C_6H_5)_4]I$ (Aldrich) were used without further purification. $(CH_3)_3SiN_3$ (Aldrich) was purified by fractional condensation prior to use. Solvents were dried by standard methods and freshly distilled prior to use. $[P(C_6H_5)_4]N_3$ and $[P(C_6H_5)_4]F$ were prepared from $[P(C_6H_5)_4]I$ and stoichiometric amounts of AgN_3 and AgF, respectively, in aqueous solution, filtering off the precipitated AgI .

Preparation of $M(N_3)_5$ (M = Nb, Ta): A sample of NbF_5 (0.55 mmol) or TaF_5 (0.59 mmol) was loaded into a Teflon-FEP ampule, followed by the addition of 1 g of SO_2 and $(CH_3)_3SiN_3$ (5.5 mmol) *in vacuo* at -196 °C. The mixture was warmed to -30 °C. After 2 hours,

the temperature was raised to -20 °C and all volatile material was pumped off, leaving behind solid $M(N_3)_5$.

$Nb(N_3)_5$: 0.175 g, expected for 0.55 mmol: 0.166 g; Raman (-80 °C): $\tilde{\nu}$=2155 [10.0], 2106 [5.5], (ν_{as} N_3), 1385 [1.6], (ν_s N_3), 628 [0.7], 590 sh, (δ N_3), 427 sh, (ν_{as} NbN_2 *eq*), 413 [3.2], (ν_s NbN_3 *eq*), 360 sh, (ν_s NbN_2 *ax*), 288 [0.7] (δ_{sciss} NbN_3 *eq*), 234 [0.7] (ρ NbN_2 *ax*); infrared (KBr): 2124 vs, 2088 vs, (ν_{as} N_3), 1374 m, 1347 s, (ν_s N_3), 591 mw, 569 w, (δ N_3), 450 sh, (ν_{as} NbN_3 *eq*), 440 mw, ($\nu_{\alpha s}$ NbN_2 *ax*), 422 w, (ν_{as} NbN_2 *eq*).

$Ta(N_3)_5$: 0.247 g, expected for 0.59 mmol = 0.231 g). Raman (-80 °C): $\tilde{\nu}$=2182 [10.0], 2129 [3.3], (ν_{as} N_3), 623 [1.1], 590 sh, (δ N_3), 450 sh, (ν_{as} TaN_2 *eq*), 426 [2.5], (ν_s TaN_3 *eq*), 390 sh, (ν_s TaN_2 *ax*), 256 [1.7] (δ $_{sciss}$ TaN_3 *eq*), 221 [2.0] (ρ TaN_2 *ax*); infrared (KBr): 2141 vs, 2103vs, (ν_{as} N_3), 1403 ms, 1364 m, (ν_s N_3), 613 mw, 578 w, (δ N_3), 410 mw, ($\nu_{\alpha s}$ TaN_2 *ax*).

In addition to these bands, the following weak infrared bands were observed which are attributed to overtones or combination bands: $Nb(N_3)_5$: 1667 w, 1263 w, 1195 sh, 1176 w, 1037 vvw, 696 w, 660 w; $Ta(N_3)_5$: 1669 w, 1508 vw, 1274 sh, 1252 w, 1203 w, 1180 sh, 1036 vw, 850 w, 712 w, 683 w.

Preparation of $CH_3CN{\cdot}M(N_3)_5$ (M = Nb, Ta): A sample of NbF_5 (0.39 mmol) or TaF_5 (0.37 mmol) was loaded into a Teflon-FEP ampule, followed by the addition of 2 mL CH_3CN and $(CH_3)_3SiN_3$ (3.7 mmol) *in vacuo* at -196 °C. The mixture was warmed to -20 °C. After 2 hours, all volatile material was pumped off at this temperature, leaving behind solid $CH_3CN{\cdot}M(N_3)_5$.

$CH_3CN{\cdot}Nb(N_3)_5$: 0.129 g, expected for 0.39 mmol: 0.136 g. Raman (-80 °C): $\tilde{\nu}$=2928 [1.8], (ν_sCH_3), 2315 [1.2], 2289 [1.1], (νCN), 2140 [10.0], 2121 [1.5], 2097 [1.9], 2090 [1.6], 2074 [2.2], 2058 [1.4], (ν_{as} N_3), 1415 [1.3], 1363 [1.2], 1351 [1.1], 1331 [1.1], (δ CH_3) and (ν_s

N_3), 947 [1.0], (νCC), 620 [1.2], 610 [1.0], 599 [1.2], 580 [1.1], 566 [1.0], 557 [1.1], (δ N_3), 441 [3.1], 435 [2.8], 423 [1.7], 419 [1.7], 411 [2.0], (ν NbN_x), 281 [1.1], 266 [1.3], 256 [1.3], 248 [1.4], 226 [1.6], (δ NbN_x) 189 [1.3], 180 [1.3], 139 [1.6], 96 [2.9] (torsional modes).

$CH_3CN{\cdot}Ta(N_3)_5$: 0.175 g, expected for 0.37 mmol: 0.161 g. Raman (-80 °C): $\tilde{\nu}$=2933 [1.7], ($\nu_s CH_3$), 2319 [0.5], 2291 [0.5], (νCN), 2172 [10.0], 2162 [1.2], 2123 [1.2], 2103 [1.1], (ν_{as} N_3), 1389 [0.4], 1361 [0.4], (δ CH_3) and (ν_s N_3), 948 [1.0], (νCC), 592 [0.3], (δ N_3), 438 [2.1], 417 [0.6], (ν NbN_x), 250 [0.7 266 [1.3], 226 [0.6], (δ NbN_x), 192 [0.9], (torsional mode).

Preparation of $[M(N_3)_6]^-$ salts (M = Nb, Ta): Neat PPh_4N_3 (0.25 mmol) was added to a frozen solution of $M(N_3)_5$ (0.25 mmol) in CH_3CN (15 mmol) at –78 °C. The reaction mixture was warmed to -25 °C and occasionally agitated. After 2 hours, all volatiles were removed at ambient temperature in a dynamic vacuum, leaving behind the solid $[M(N_3)_6]^-$ salts.

$[P(C_6H_5)_4][Nb(N_3)_6]$: orange solid, 0.160 g, expected for 0.25 mmol: 0.171 g. The IR and Raman spectra of $Nb(N_3)_6^-$ are given in Table1.

$[P(C_6H_5)_4][Ta(N_3)_6]$: pale yellow solid, 0.207 g, expected for 0.25 mmol: 0.193 g. Raman bands due to $[Ta(N_3)_6]^-$ (-80 °C): $\tilde{\nu}$=2159 [10.0], 2111 [1.0], 2103 [1.0], 2091 [0.8], 2081 [0.7], (ν_{as} N_3), 1355 [0.8], (ν_s N_3), 609 [0.6], 582 [0.4], (δ N_3), 437 [2.8], 372 [0.7], 364 [0.8], 353 [0.8], (ν TaN_6), 225 [1.8], 215 [1.8], (δ TaN_6), 168 [2.6], 160 [2.6], (torsions); infrared bands due to $[Ta(N_3)_6]^-$ (KBr): 2124 vs, 2113 vs, 2096 vs, 2087 vs, (ν_{as} N_3), 1383 m, 1372 m, 1360 ms, 1348 s, (ν_s N_3), 648 vw, 615 m, 600 mw, 585 mw, 576 w, (δ N_3), 433 w, 418 mw, 414 mw, (ν TaN_6).

Theoretical Methods: The molecular structures, harmonic vibrational frequencies, and infrared and Raman vibrational intensities were calculated using second order perturbation theory (MP2, also known as MBPT(2)[24]) and also at the DFT level using the B3LYP hybrid functional,[23a]

which included the VWN5 correlation functional.[23b] The Stevens, Basch, Krauss, and Jasien (SBKJ) effective core potentials and the corresponding valence-only basis sets were used.[25a] The SBKJ valence basis set for nitrogen was augmented with a d polarization function[25b] and a diffuse s+p shell,[25c] denoted as SBKJ+(d). Hessians (energy second derivatives) were calculated for the final equilibrium structures to verify them as local minima; i.e., having a positive definite Hessian. All calculations were performed using the electronic structure code GAMESS.[45]

Received: , 2004

Keywords: Crystal structure, hexaazidoniobate(V), hexaazidotantalate(V), niobium pentaazide, niobium pentaazide - acetonitrile adduct, tantalum pentaazide, tantalum pentaazide – acetonitrile adduct, vibrational spectra, binary Group 5 azides, theoretical calculations, linear metal-nitrogen-nitrogen bonds, rule of 12

References

[1] R. Haiges, J. A. Boatz, S. Schneider, T. Schroer, K. O. Christe, *Angew. Chem. Int. Ed*. **2004**, *43,* 3148.

[2] R. Haiges, J. A. Boatz, R. Bau, S. Schneider, T. Schroer, M. Yousufuddin, K. O. Christe, *Angew. Chem. Int. Ed. submitted*.

[3] A. Kornath, *Angew. Chem. Int. Ed.* **2001**, *40*, 3135 and references cited therein.

[4] K. Dehnicke, J. Strähle, *Z. Anorg. Allg. Chem.* **1965**, *338*, 287.

[5] K. Dehnicke, *J. Inorg. Nucl. Chem.* **1965**, *27*, 809.

[6] J. Strähle, *Z. Anorg. Allg. Chem.* **1974**, *405*, 139.

[7] R. Choukroun, D. Gervais, *J. Chem. Soc., Dalton Trans.* **1980**, 1800.

[8] U. Müller, R. Dübgen, K. Dehnicke, *Z. Anorg. Allg. Chem.* **1981**, *473*, 115.

[9] a) W. Beck, E. Schuierer, P. Poellmann, W. P. Fehlhammer, *Z. Naturforsch. B*, **1966**, *21*, 811; b) W. Beck, W. P. Fehlhammer, P. Poellmann, E. Schuierer, K. Feldl, *Chem. Ber.* **1967**, *100*, 2335.

[10] D. B. Sable, W. H. Armstrong, *Inorg. Chem*. **1992**, *31*, 161.

[11] J. H. Espenson, J. R. Pladziewicz, *Inorg. Chem.* **1970**, *9*, 1380.

[12] M. Kasper, R. Bereman, *Inorg. Nucl. Chem. Let*. **1974**, *10*, 443.

[13] M. Herberhold, A.-M. Dietel, W. Milius, *Z. Anorg. Allg. Chem.* **1999**, *625*, 1885.

[14] J. H. Osborne, A. L. Rheingold, W. C. Trogler, *J. Am. Chem. Soc.* **1985**, *107*, 7945.

[15] M. Herberhold, A. Goller, W. Milius, *Z. Anorg. Allg. Chem.* **2003**, *629*, 1162.

[16] M. Herberhold, A. Goller, W. Milius, *Z. Anorg. Allg. Chem.* **2003**, *629*, 1557.

[17] M. Herberhold, A. Goller, W. Milius, *Z. Anorg. Allg. Chem.* **2001**, *627*, 891.

[18] J. H. Meyer, *Z. Anorg. Allg. Chem.* **1995**, *621*, 921.

[19] O. Reckeweg, H.-J. Meyer, A. Simon, *Z. Anorg. Allg. Chem.* **2002**, *628*, 920.

[20] H.-J. Meyer, *Z. Anorg. Allg. Chem.* **1995**, *621*, 921.

[21] R. Dübgen, U. Müller, F. Weller, K. Dehnicke, *Z. Anorg. Allg. Chem.* **1980**, *471*, 89.

[22] A. M. Golub, H. Köhler, V. V. Stopenko, *Chemistry of Pseudohalides*, Elsevier, Amsterdam, **1986**.

[23] a) A. D. Becke, *J. Chem. Phys*. **1993**, *98*, 5648; P. J. Stephens, F. J. Devlin, C. F. Chablowski, M. J. Frisch, *J. Phys. Chem*. **1994,** 98, 11623; R. H. Hertwig, W. Koch, *Chem. Phys. Lett*. **1997**, 268, 345.

b) S. H. Vosko, L. Wilk, M. Nusair, *Can. J. Phys.* **1980**, 58, 1200.

[24] C. Moller, M. S. Plesset, *Phys. Rev.* **1934,** *46,* 618; J. A. Pople, J. S. Binkley, R. Seeger, *Int. J. Quantum Chem. S10,* **1976**, 1; M. J. Frisch, M. Head-Gordon, J. A. Pople, *Chem.Phys.Lett.* **1990**, *166*, 275; . J. Bartlett, D. M. Silver, *Int. J. Quantum Chem. Symp.* **1975,** *9,* 1927.

[25] a) W. J. Stevens, H. Basch, M. Krauss, *J. Chem. Phys.* **1984,** *81*, 6026; W. J. Stevens, M. Krauss, H. Basch, P. G. Jasien, *Can. J. Chem.* **1992,** 70, 612.

b) P. C. Hariharan, J. A. Pople, *Theoret. Chim. Acta* **1973,** *28*, 213.

c) T. Clark, J. Chandrasekhar, G. W. Spitznagel, P. von R. Schleyer, *J. Comput. Chem.* **1983,** *4*, 294.

[26] J. Drummond, J. S. Wood, *J. Chem. Soc., Chem. Commun.*. **1969,** 1373.

[27] R. Haiges, J. A. Boatz, A. Vij, V. Vij, M. Gerken, S. Schneider, T. Schroer, M. Yousufuddin, K. O. Christe, *Angew. Chem. Int. Ed*. **2004**, *43,* in press.

[28] a) K. Karaghiosoff, T. M. Klapötke, B. Krumm, H. Nöth, T. Schütt, M. Suter, *Inorg. Chem.* **2002**, *41*, 170; b) T. M. Klapötke, H. Nöth, T. Schütt, M. Warchhold, *Angew. Chem. Int. Ed.* **2000**, *39*, 2108.

[29] (a) R. J. Gillespie, I. Hargittai, *The VSEPR Model of Molecular Geometry,* Allyn and Bacon, A Division of Simon & Schuster, Inc.: Needham Heights, MA, **1991**; (b) R. J. Gillespie, P. L. A. Popelier, *Chemical Bonding and Molecular Geometry: from Lewis to Electron Densities,* Oxford University Press, **2001**.

[30] L. Gagliardi, P. Pyykkoe, *Inorg. Chem.* **2003,** *42,* 3074.

[31] U. Mueller, H. Baernighausen, *Acta Crystallogr.***1970,** *B26,*1671.

[32] W. Fraenk, T. Habereder, A. Hammerl, T. M. Klapoetke, B. Krumm, P. Mayer, H. Noeth, M. Warchhold, *Inorg. Chem.* **2001,** *40,* 1334.

[33] T. M. Klapoetke, H. Noeth, T. *Angew. Chem. Int. Ed*. **2000**, *39,* 2108.

[34] R. Haiges, J. A. Boatz, A. Vij, M. Gerken, S. Schneider, T. Schroer, K. O. Christe, *Angew. Chem. Int. Ed*. **2003**, *42,* 5847.

[35] P. Nockemann, U. Cremer, U. Ruschewitz, G. Meyer, *Z. Anorg. Allg. Chem.* **2003**, *629*, 2079.

[36] J. O. Jensen, *Vibr. Spectrosc.* **2003,** *31,* 227.

[37] Crystal data for $C_2H_3N_{16}Nb$: M_r = 344.11, monoclinic, space group $P2(1)/c$, a = 7.9805(12), b = 10.4913(16), c = 14.695(2) Å, α = 90, β = 96.353(2), γ = 90°, V = 1222.8(3) Å^3, $F(000)$ = 672, $\rho_{calcd.}$ (Z = 4) = 1.869 g·cm^{-3}, μ = 1.004 mm^{-1}, approximate crystal dimensions 0.25 x 0.08 x 0.02 mm^3, θ range = 2.39 to 27.48°, $Mo_{K\alpha}$ (λ = 0.71073 Å), T = 163(2) K, 3392 measured data (Bruker 3-circle, SMART APEX CCD with χ-axis fixed at 54.74°, using the SMART V 5.625 program, Bruker AXS: Madison, WI, 2001), of which 839 (R_{int} = 0.0204) unique. Lorentz and polarization correction (SAINT V 6.22 program, Bruker AXS: Madison, WI, 2001), absorption correction (SADABS program, Bruker AXS: Madison, WI, 2001). Structure solution by direct methods (SHELXTL 5.10, Bruker AXS: Madison, WI, 2000), full-matrix least-squares refinement on F^2, data to parameters ratio: 15.9 : 1, final R indices [$I>2\sigma(I)$]: $R1$ = 0.0341, $wR2$ = 0.0692, R indices (all data): $R1$ = 0.0546, $wR2$ = 0.0746, GOF on F^2 = 1.003. Further crystallographic details can be obtained from the Cambridge Crystallographic Data Centre (CCDC, 12 Union Road, Cambridge CB21EZ, UK (Fax: (+44) 1223-336-033; e-mail: deposit@ccdc.cam.ac.uk) on quoting the deposition no. CCDC 246594.

[38] B. v. Ahsen, B. Bley, S. Proemmel, R. Wartchow, H. Willner, F. Aubke, *Z. Anorg. Allg. Chem.* **1998**, *624*, 1225.

[39] D. M. Byler, D. F. Shriver, *Inorg. Chem.* **1973,** *12,* 1412 and **1974,** *13,* 2697 .

[40] Crystal data for $C_{24}H_{20}N_{18}NbP$: M_r = 684.46, orthorhombic, space group *P*2(1)2(1)2, a = 18.480(3), b = 23.153(4), c = 6.7831(13) Å, α = 90, β = 90, γ = 90°, V = 2902.3(9) Å^3, *F(000)* = 1384, $\rho_{calcd.}$ (Z = 4) = 1.566 g·cm^{-3}, μ = 0.521 mm^{-1}, approximate crystal dimensions 0.33 x 0.05 x 0.04 mm^3, θ range = 1.41 to 27.51°, $Mo_{K\alpha}$ (λ = 0.71073 Å), T = 133(2) K, 17936 measured data (Bruker 3-circle, SMART APEX CCD with χ-axis fixed at 54.74°, using the SMART V 5.625 program, Bruker AXS: Madison, WI, 2001), of which 6575 (R_{int} = 0.0597) unique. Lorentz and polarization correction (SAINT V 6.22 program, Bruker AXS: Madison, WI, 2001), absorption correction (SADABS program, Bruker AXS: Madison, WI, 2001). Structure solution by direct methods (SHELXTL 5.10, Bruker AXS: Madison, WI, 2000), full-matrix least-squares refinement on F^2, data to parameters ratio: 16.5 : 1, final R indices [$I>2\sigma(I)$]: *R1* = 0.0518, *wR2* = 0.0936, R indices (all data): *R1* = 0.0858, *wR2* = 0.1049, GOF on F^2 = 1.028. Further crystallographic details can be obtained from the Cambridge Crystallographic Data Centre (CCDC, 12 Union Road, Cambridge CB21EZ, UK (Fax: (+44) 1223-336-033; e-mail: deposit@ccdc.cam.ac.uk) on quoting the deposition no. CCDC 251934.

[41] J. Weidlein, U. Mueller, K. Dehnicke, *Schwingungsspektroskopie,* Georg Thieme Verlag, Stuttgart-New York, **1982,** pg. 102.

[42] A. C. Filippou, P. Portius, G. Schnakenburg, *J. Am. Chem. Soc.* **2002**, *124*, 12396.

[43] A. C. Filippou, P. Portius, D. U. Neumann, K.-D. Wehrstedt, *Angew. Chem. Int. Ed.* **2000**, *39*, 4333.

[44] K. O. Christe, W. W. Wilson, C. J. Schack, R. D. Wilson, *Inorg. Synth.* **1986**, *24*, 39.

[45] M. W. Schmidt, K. K. Baldridge, J. A. Boatz, S. T. Elbert, M. S. Gordon, J. H. Jensen, S. Koseki, N. Matsunaga, K. A. Nguyen, S. J. Su, T. L. Windus, M. Dupuis, J. A. Montgomery, *J. Comput. Chem.* **1993**, *14*, 1347.

Table 1. Comparison of observed and unscaled calculated vibrational frequencies [cm^{-1}] and intensities for $[Nb(N_3)_6]^{-}$[a] in point group S_6

	description	observed IR	Ra	Calculated (IR) [Raman] B3LYP/SBK+(d)	MP2/SBK+(d)
A_g ν_1	$\nu_{as}N_3$		2131 (10.0) 2112 (5.6)	2218 (0) [1428]	2129 (0) [1388]
ν_2	ν_sN_3		1342 (2.0)	1432 (0) [49]	1283 (0) [60]
ν_3	δN_3		616 (2.8)	588 (0) [8.8]	565 (0) [39]
ν_4	δN_3			580 (0) [2.2]	524 (0) [2.3]
ν_5	ν_sNbN_6		433 (5.3) 414 (4.8)	401 (0) [147]	402 (0) [367]
ν_6	δ_sNbN_6		225 (3.5)	249 (0) [13]	242 (0) [51]
ν_7	τ			74 (0) [14]	72 (0) [31]
ν_8	τ			34 (0) [37]	32 (0) [39]
E_g ν_9	$\nu_{as}N_3$		2080 (2.1) 2060 (2.3)	2164 (0) [1063]	2146 (0) [110]
ν_{10}	ν_sN_3			1413 (0) [50]	1279 (0) [154]
ν_{11}	δN_3			582 (0) [8.4]	550 (0) [73]
ν_{12}	δN_3			580 (0) [0.63]	521 (0) [4.2]
ν_{13}	ν_sNbN_6		339 (2.7)	334 (0) [12]	350 (0) [38]
ν_{14}	δ_sNbN_6		217 (3.5)	238 (0) [34]	234 (0) [31]
ν_{15}	τ			87 (0) [36]	89 (0) [92]
ν_{16}	τ			36 (0) [69]	38 (0) [80]
A_u ν_{17}	$\nu_{as}N_3$	2121 s 2080 vs		2185 (4084) [0]	2152 (2577) [0]
ν_{18}	ν_sN_3	1336 ms		1406 (677) [0]	1271 (338) [0]
ν_{19}	δN_3	640 vw		580 (0.91) [0]	549 (100) [0]
ν_{20}	δN_3	624 w		574 (49) [0]	505 (8.0) [0]
ν_{21}	$\nu_{as}NbN_6$	409 mw		400 (536) [0]	418 (629) [0]
ν_{22}	$\delta_{as}NbN_6$			276 (15) [0]	262 (31) [0]
ν_{23}	τ NbN_6			140 (2.8) [0]	114(0.48) [0]
ν_{24}	τ			27 (0.006) [0]	29 (0.022) [0]
ν_{25}	τ			24 (1.6) [0]	14 (0.37) [0]
E_u ν_{26}	$\nu_{as}N_3$	2069 vs 2060 vs		2170 (4366) [0]	2141 (2681) [0]
ν_{27}	ν_sN_3	1361 m 1351 m		1409 (739) [0]	1278 (314) [0]
ν_{28}	δN_3	600 w		577 (126) [0]	544 (94) [0]
ν_{29}	δN_3	583 vw		570 (38) [0]	502 (8.2) [0]
ν_{30}	$\nu_{as}NbN_6$	409 mw	382 (2.8)	391 (874) [0]	404 (1045) [0]
ν_{31}	$\delta_{as}NbN_6$			233 (26) [0]	223 (30) [0]
ν_{32}	$\delta_{wag/rock}NbN_6$		151 (4.3)	154 (13) [0]	128 (31) [0]
ν_{33}	τ			36 (4.8) [0]	38 (3.1) [0]
ν_{34}	τ			15 (1.6) [0]	6 (1.9) [0]

[a] Calculated IR and Raman intensities are given in km mol^{-1} and $Å^4$ amu^{-1}, respectively; observed spectra are for the solid $[P(C_6H_5)_4]^+$ salt.

Figure 1. IR and Raman spectrum of solid $Nb(N_3)_5$. The band marked by an asterisk (*) is due to the Teflon-FEP sample tube.

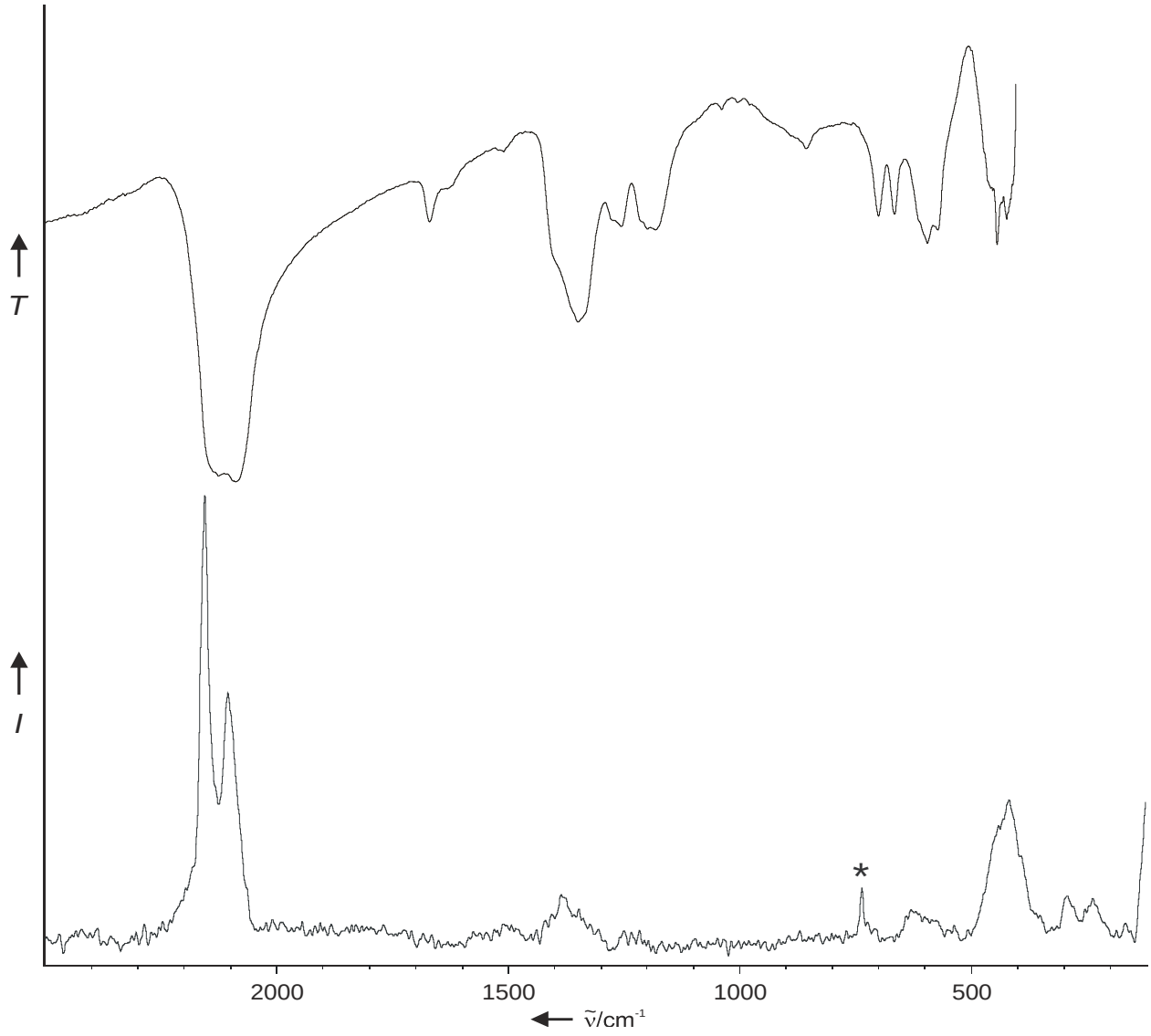

Figure 2. IR and Raman spectra of $Ta(N_3)_5$. The band marked by an asterisk (*) is due to the Teflon-FEP sample tube.

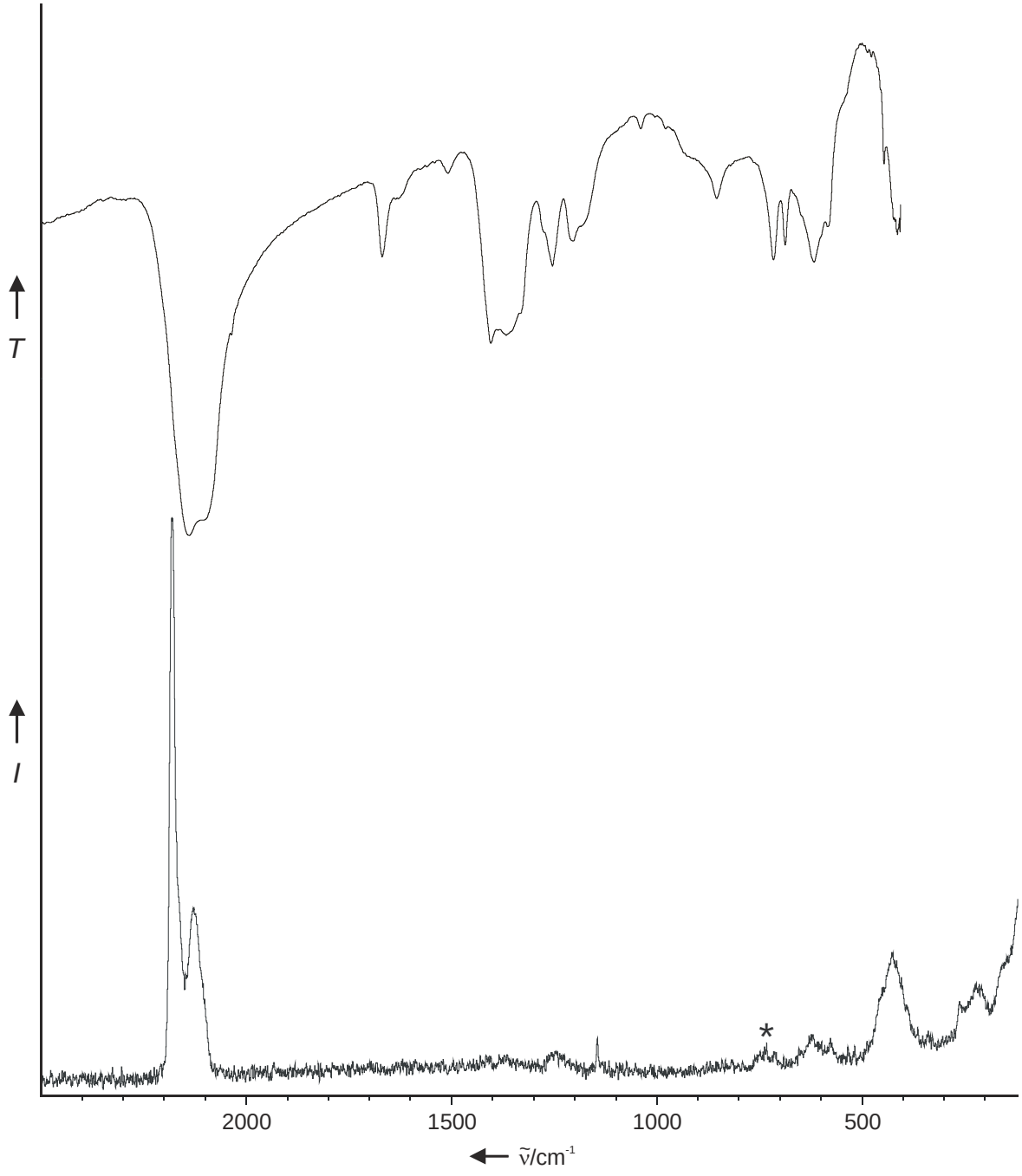

Figure 3. Stuctures of $Nb(N_3)_5$ and $Ta(N_3)_5$ calculated at the B3LYP/SBKJ+(d) level of theory (MP2/SBKJ+(d) values in parentheses.)

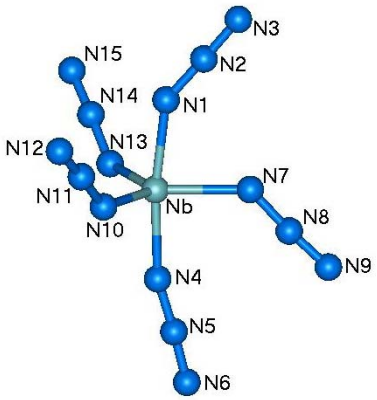

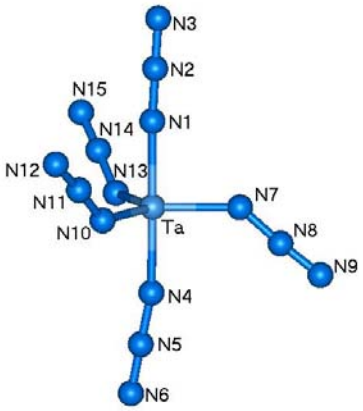

$R(Nb-N_1)$ = 2.025(2.013)	$R(Ta-N_1)$ = 1.997(1.996)
$R(Nb-N_4)$ = 2.001(2.002)	$R(Ta-N_4)$ = 1.991(1.993)
$R(Nb-N_7)$ = 2.048(2.060)	$R(Ta-N_7)$ = 2.003(1.997)
$R(Nb-N_{10})$ = 2.008(2.014)	$R(Ta-N_{10})$ = 2.008(2.009)
$R(Nb-N_{13})$ = 2.008(2.014)	$R(Ta-N_{13})$ = 2.008(2.009)
$R(N_1-N_2)$ = 1.234(1.241)	$R(N_1-N_2)$ = 1.226(1.235)
$R(N_4-N_5)$ = 1.230(1.241)	$R(N_4-N_5)$ = 1.225(1.234)
$R(N_7-N_8)$ = 1.243(1.249)	$R(N_7-N_8)$ = 1.240(1.242)
$R(N_{10}-N_{11})$ = 1.240(1.245)	$R(N_{10}-N_{11})$ = 1.240(1.244)
$R(N_{13}-N_{14})$ = 1.240(1.245)	$R(N_{13}-N_{14})$ = 1.240(1.244)
$R(N_2-N_3)$ = 1.162(1.208)	$R(N_2-N_3)$ = 1.163(1.209)
$R(N_5-N_6)$ = 1.163(1.210)	$R(N_5-N_6)$ = 1.163(1.209)
$R(N_8-N_9)$ = 1.162(1.210)	$R(N_8-N_9)$ = 1.160(1.206)
$R(N_{11}-N_{12})$ = 1.160(1.208)	$R(N_{11}-N_{12})$ = 1.160(1.206)
$R(N_{14}-N_{15})$ = 1.160(1.208)	$R(N_{14}-N_{15})$ = 1.160(1.206)
$\alpha(N_1-Nb-N_4)$ = 171.9(169.0)	$\alpha(N_1-Ta-N_4)$ = 179.2(177.9)
$\alpha(N_1-Nb-N_7)$ = 82.8(81.4)	$\alpha(N_1-Ta-N_7)$ = 89.4(90.2)
$\alpha(N_1-Nb-N_{10})$ = 91.0(92.1)	$\alpha(N_1-Ta-N_{10})$ = 90.2(89.8)
$\alpha(N_1-Nb-N_{13})$ = 91.0(92.1)	$\alpha(N_1-Ta-N_{13})$ = 90.2(89.8)
$\alpha(N_4-Nb-N_7)$ = 89.1(87.6)	$\alpha(N_4-Ta-N_7)$ = 91.4(91.8)
$\alpha(N_4-Nb-N_{10})$ = 93.2(93.6)	$\alpha(N_4-Ta-N_{10})$ = 89.4(89.2)
$\alpha(N_4-Nb-N_{13})$ = 93.2(93.6)	$\alpha(N_4-Ta-N_{13})$ = 89.4(89.2)
$\alpha(N_7-Nb-N_{10})$ = 121.3(121.3)	$\alpha(N_7-Ta-N_{10})$ = 119.6(119.1)
$\alpha(N_7-Nb-N_{13})$ = 121.3(121.3)	$\alpha(N_7-Ta-N_{13})$ = 119.6(119.1)
$\alpha(N_{10}-Nb-N_{13})$ = 117.2(117.1)	$\alpha(N_{10}-Ta-N_{13})$ = 120.9(121.7)
$\alpha(Nb-N_1-N_2)$ = 145.3(147.2)	$\alpha(Ta-N_1-N_2)$ = 176.9(178.5)
$\alpha(Nb-N_4-N_5)$ = 165.0(157.3)	$\alpha(Ta-N_4-N_5)$ = 169.3(173.8)
$\alpha(Nb-N_7-N_8)$ = 131.8(130.8)	$\alpha(Ta-N_7-N_8)$ = 137.7(143.0)
$\alpha(Nb-N_{10}-N_{11})$ = 137.2(138.8)	$\alpha(Ta-N_{10}-N_{11})$ = 137.1(138.9)
$\alpha(Nb-N_{13}-N_{14})$ = 137.2(138.8)	$\alpha(Ta-N_{13}-N_{14})$ = 137.1(138.9)

Figure 4. Bonding schemes for transition metal azides (from top to bottom): (i) ionic azide, showing for didactic reasons the azide ion in one of its asymmetric resonance structures and only some of the empty s^2d^{10} orbitals on M; (ii) strongly bent two-center/monodative bond; (iii) moderately bent two-center/bidative bond; (iv) linear two-center/tridative bond.

IONIC
M^+ N_3^-

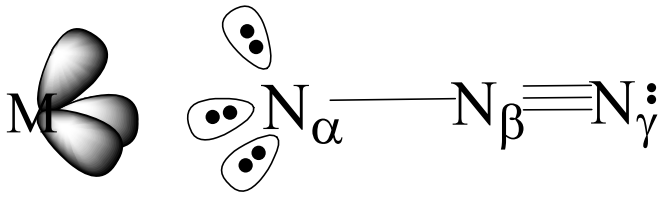

2c-1d
$\angle(M–N_\alpha–N_\beta) = 109.5^o$

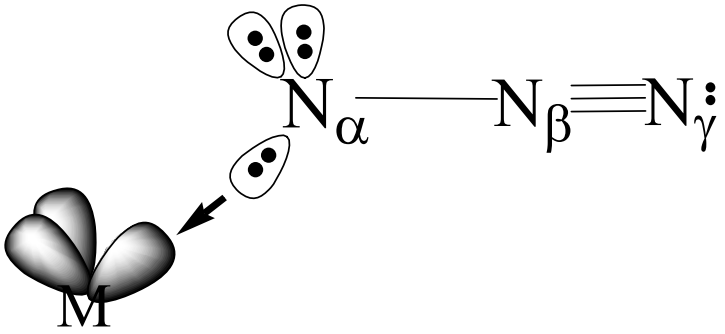

2c-2d
$\angle(M–N_\alpha–N_\beta) = 125.5^o$

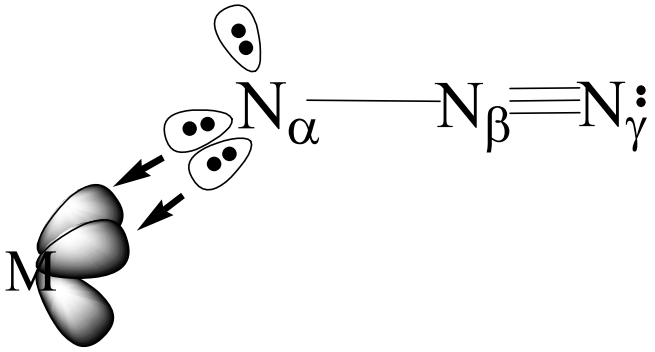

2c-3d
$\angle(M–N_\alpha–N_\beta) = 180.0^o$

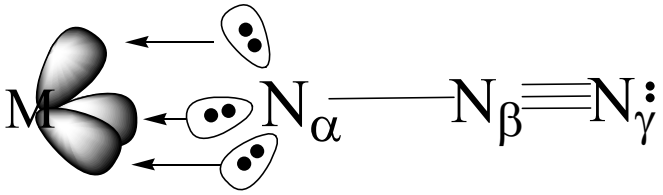

Figure 5. Raman spectrum of solid $CH_3CN{\cdot}Nb(N_3)_5$. The band marked by an asterisk (*) is due to the Teflon-FEP sample tube.

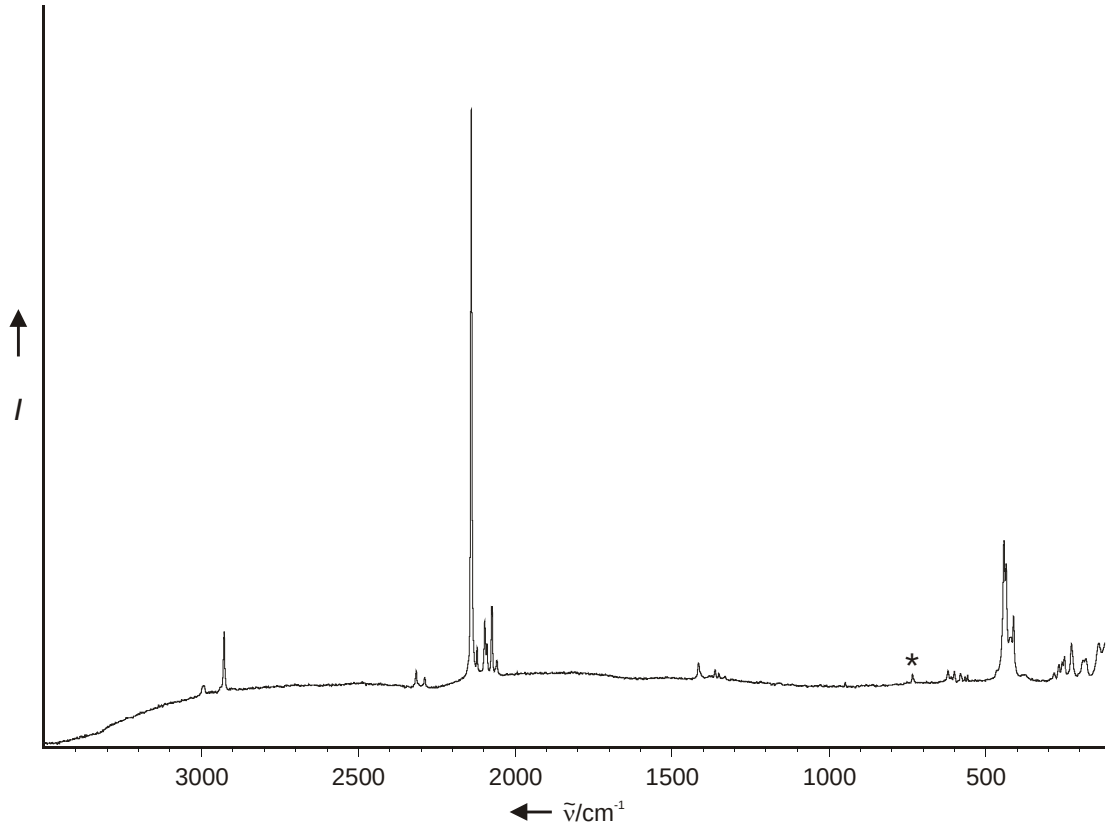

Figure 6. Raman spectrum of solid $CH_3CN \cdot Ta(N_3)_5$. The band marked by an asterisk (*) is due to the Teflon-FEP sample tube.

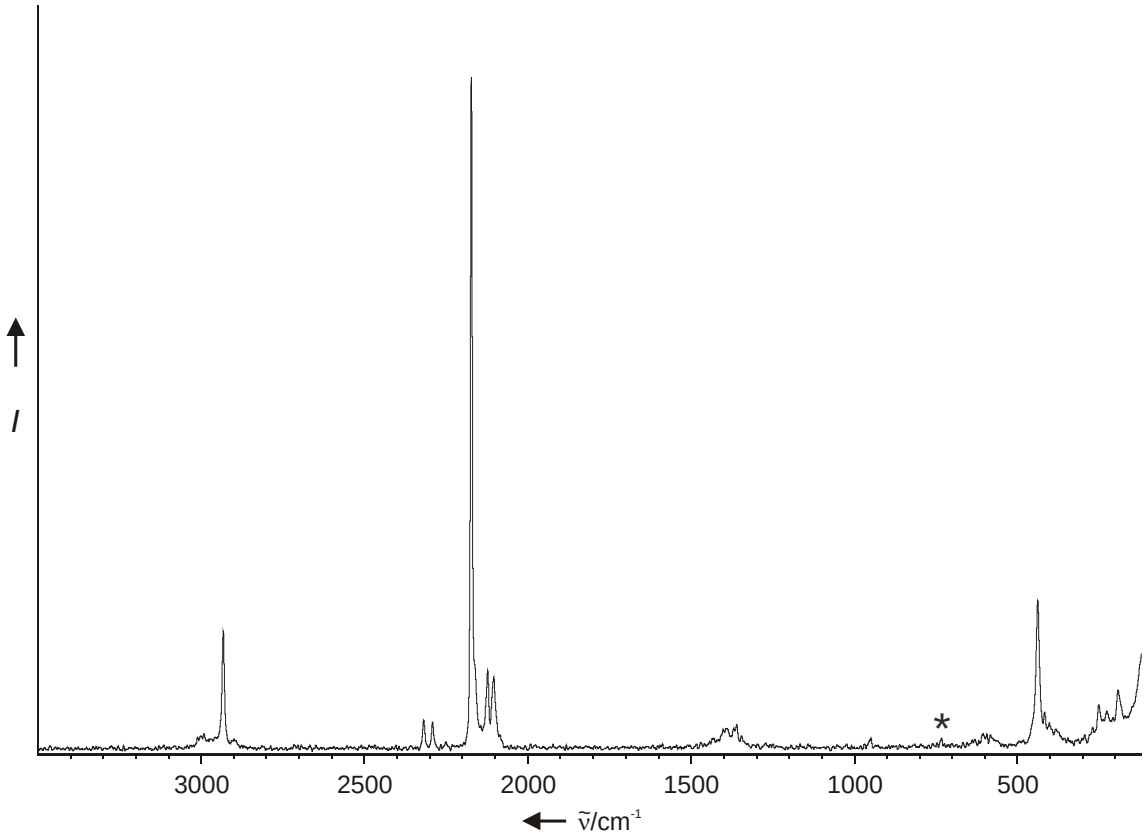

Figure 7. ORTEP drawing of $CH_3CN{\cdot}Nb(N_3)_5{\cdot}$. Thermal ellipsoids are shown at the 50% probability level. Selected bond lengths [Å] and angles [°]: Nb-N1 2.031(3), Nb-N4 1.998(3), Nb-N7 2.004(3), Nb-N10 2.017(3), Nb-N13 1.935(3), Nb-N16 2.259(3), N1-N2 1.217(4), N2-N3 1.139(4), N4-N5 1.212(4), N5-N6 1.133(4), N7-N8 1.212(4), N8-N9 1.129(4), N10-N11 1.211(4), N11-N12 1.132(4), N13-N14 1.205(4), N14-N15 1.137(4), N16-C1 1.139(4), C1-C2 1.447(5), N1-Nb-N4 87.55(12), N1-Nb-N7 165.51(11), N1-Nb-N10 82.89(12), N1-Nb-N13 99.16(12), N1-Nb-N16 84.59(10), N4-Nb-N7 93.90(12), N4-Nb-N10 162.91(12), N4-Nb-N13 96.38(12), N4-Nb-N16 81.15(10), N7-Nb-N10 91.93(11), N7-Nb-N13 95.01(12), N7-Nb-N16 81.40(11), N10-Nb-N13 99.11(12), N10-Nb-N16 83.86(10), N13-Nb-N16 175.45(11), Nb-N1-N2 132.7(2), Nb-N4-N5 141.9(2), Nb-N7-N8 144.1(2), Nb-N10-N11 132.3(2), Nb-N13-N14 168.8(2).

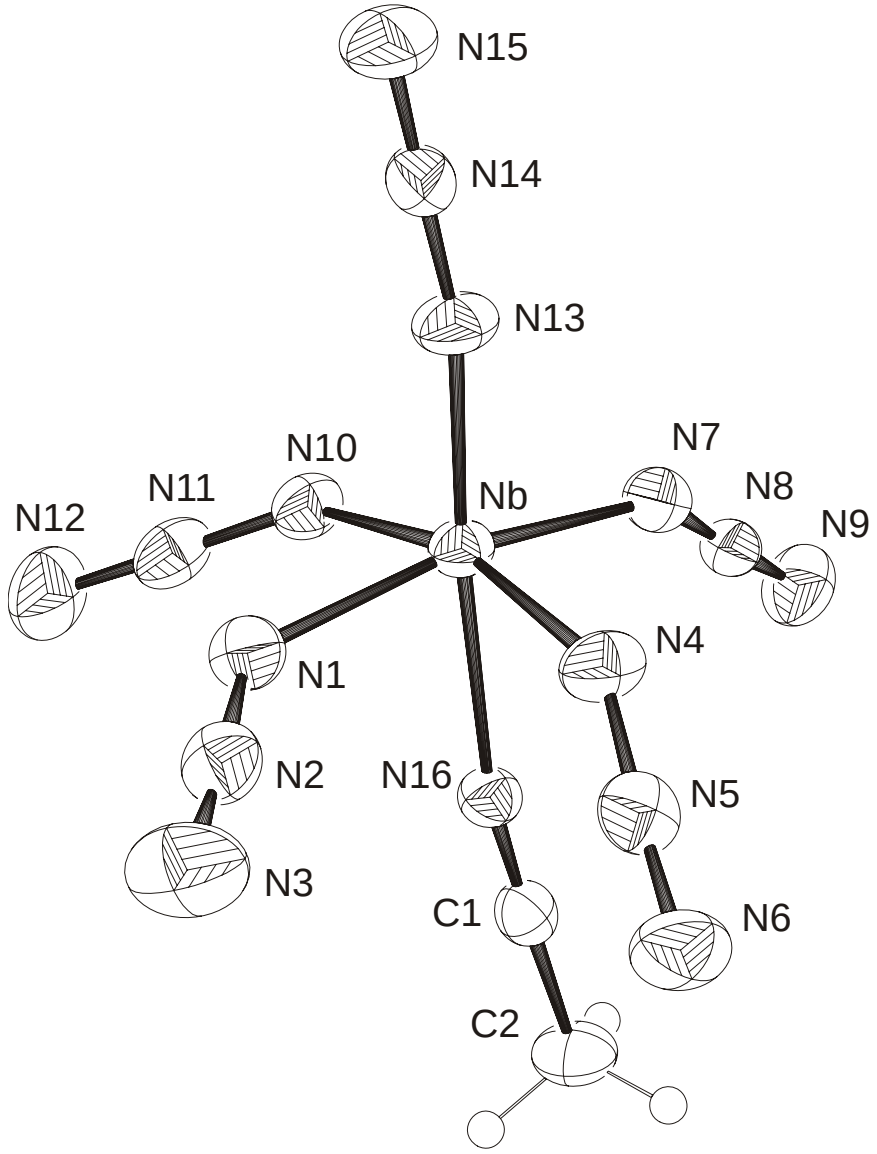

Figure 8. IR and Raman spectra of $[PPh_4][Nb(N_3)_6]$. The bands belonging to the $[Nb(N_3)_6]^-$ ion are marked with a diamond (♦).

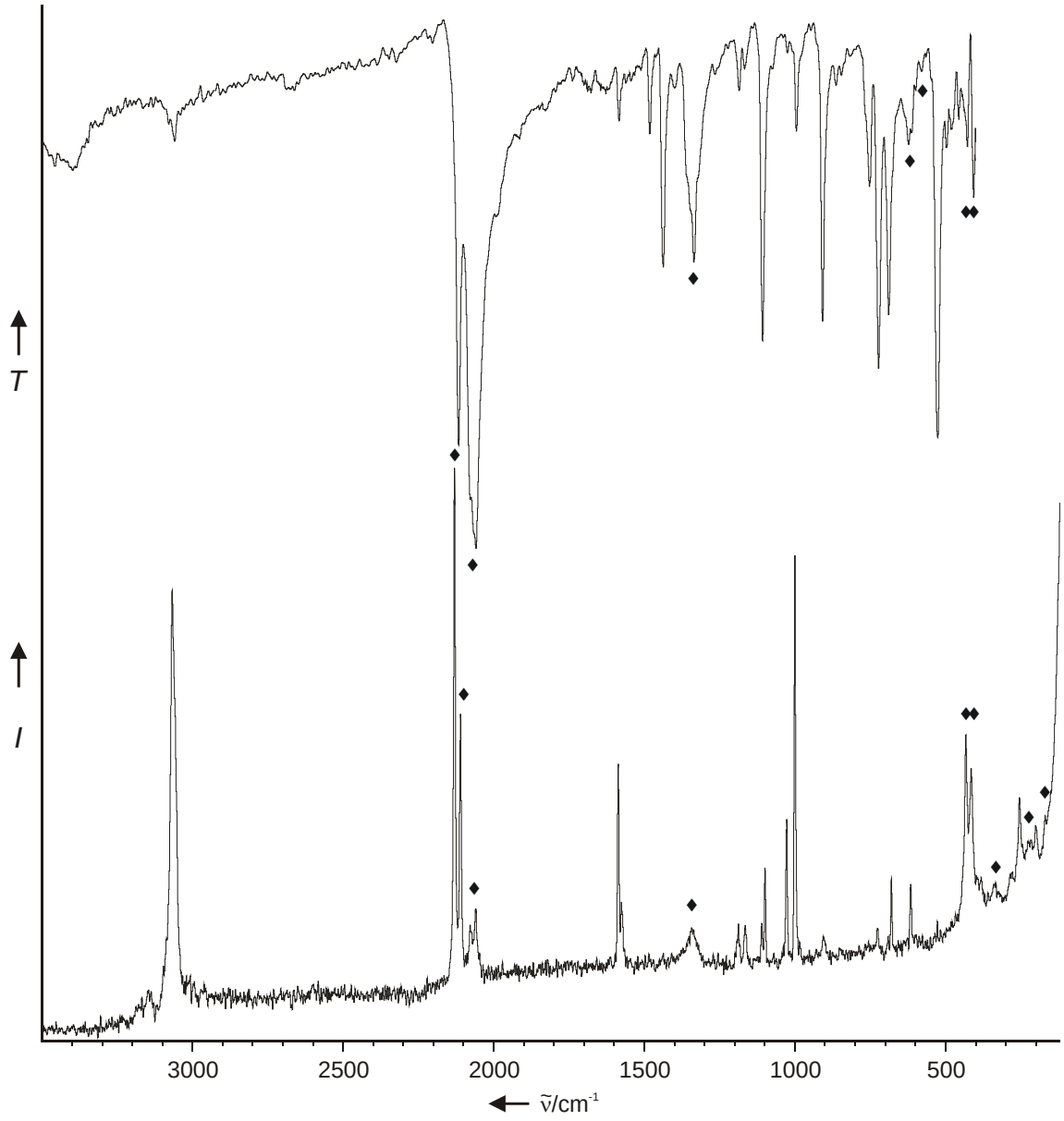

Figure 9. IR and Raman spectra of $[PPh_4][Ta(N_3)_6]$. The bands belonging to the $[Ta(N_3)_6]^-$ ion are marked with a diamond (♦). The band marked by an asterisk (*) is due to the Teflon-FEP sample tube.

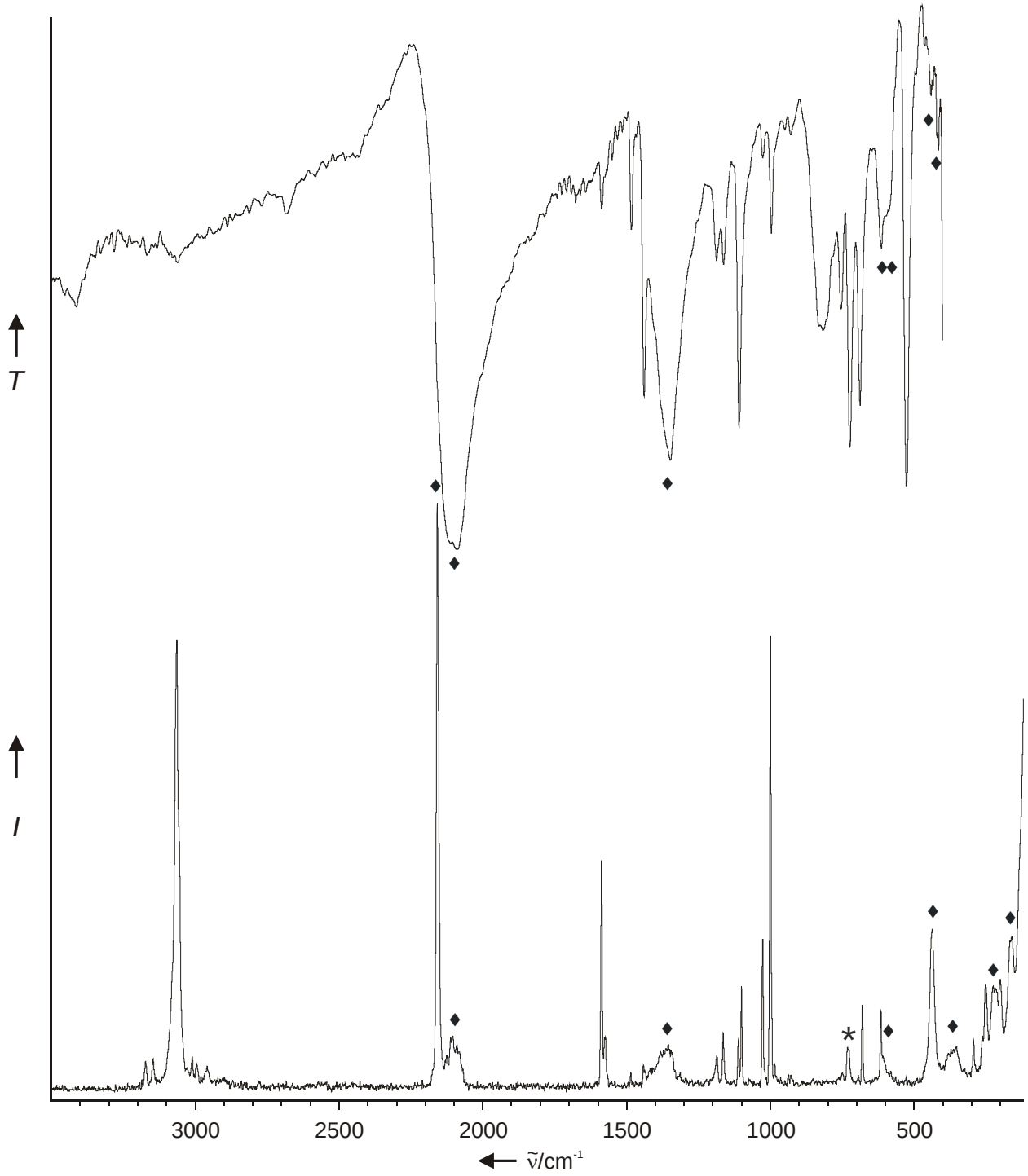

Figure 10. ORTEP drawing of the anionic part of the crystal structure of $[P(C_6H_5)_4][Nb(N_3)_6]$. Thermal ellipsoids are shown at the 50% probability level. Selected bond lengths [Å] and angles [°]: Nb-N1 2.078(5), Nb-N4 2.035(4), Nb-N7 1.989(4), Nb-N10 2.008(4), Nb-N13 2.032(4), Nb-N16 2.026(5), N1-N2 1.164(5), N2-N3 1.126(6), N4-N5 1.198(5), N5-N6 1.128(5), N7-N8 1.192(5), N8-N9 1.133(5), N10-N11 1.196(5), N11-N12 1.118(5), N13-N14 1.203(6), N14-N15 1.137(6), N16-N17 1.173(6), N17-N18 1.137(6), N1-Nb-N4 89.54(19), N1-Nb-N7 173.25(18), N1-Nb-N10 94.23(18), N1-Nb-N13 80.45(18), N1-Nb-N16 85.2(2), N4-Nb-N7 86.30(18), N4-Nb-N10 174.15(18), N4-Nb-N13 95.40(15), N4-Nb-N16 86.78(17), N7-Nb-N10 90.34(17), N7-Nb-N13 94.63(17), N7-Nb-N16 99.86(19), N10-Nb-N13 89.63(18), N10-Nb-N16 89.1(2), N13-Nb-N16 165.46(18), Nb-N1-N2 134.4(4), Nb-N4-N5 141.2(4), Nb-N7-N8 156.2(4), Nb-N10-N11 152.3(4), Nb-N13-N14 131.7(4), Nb-N16-N17 142.3(4).

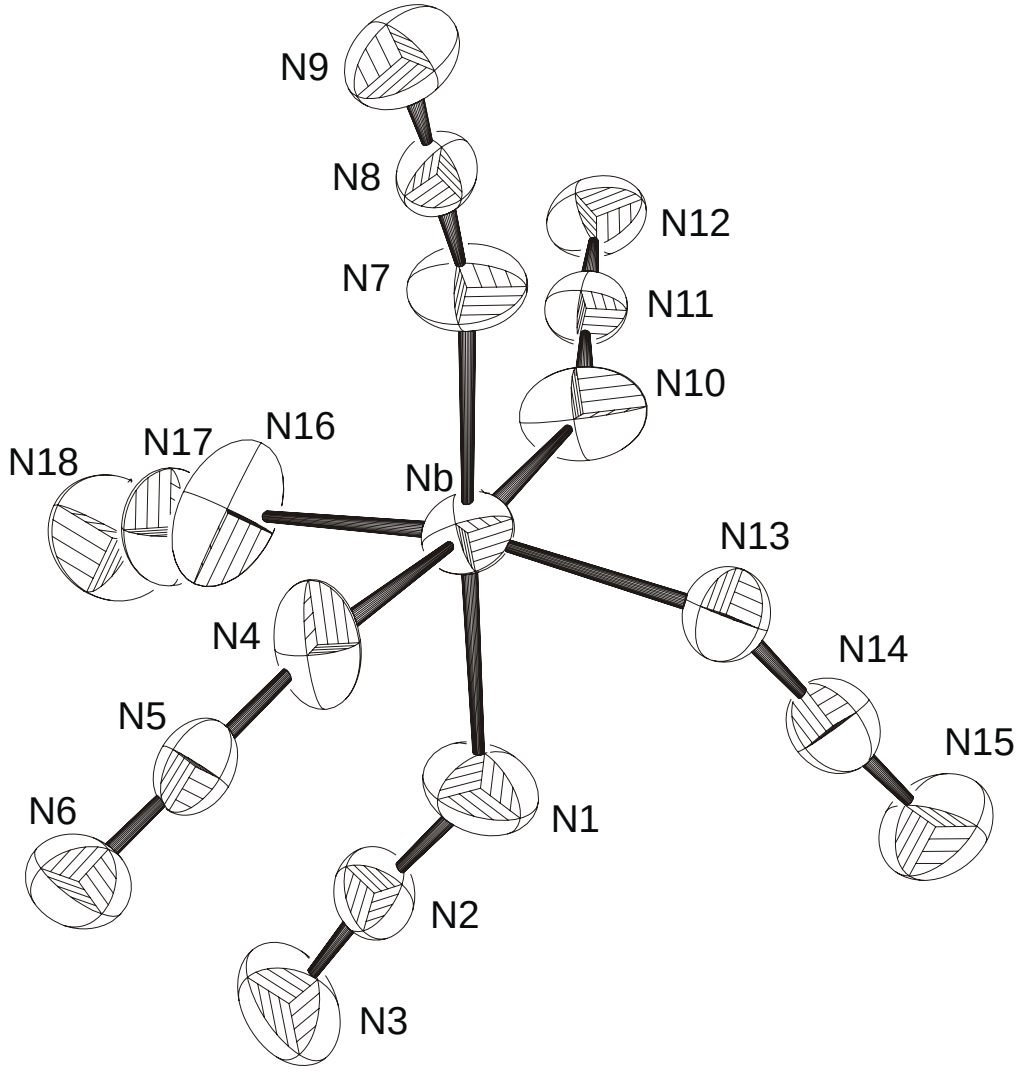

Synopsis

R. Haiges*, Jerry A. Boatz, T. Schroer, Muhammed Yousufuddin, K. O. Christe*

Experimental Evidence for Linear Metal-Azide Bonds. The Binary Group 5 Azides $Nb(N_3)_5$, $Ta(N_3)_5$, $[Nb(N_3)_6]^-$ and $[Ta(N_3)_6]^-$, and 1:1 Adducts of $Nb(N_3)_5$ and $Ta(N_3)_5$ with CH_3CN

The first examples of binary azides with linear metal-N-N bonds have been prepared and characterized. The occurrence of linear metal-N-N bonds can be explained by the α-nitrogen atom of the azido group acting as a tridative ligand and the tendency of the transition metal centers seeking a filled s^2d^{10} electron shell.

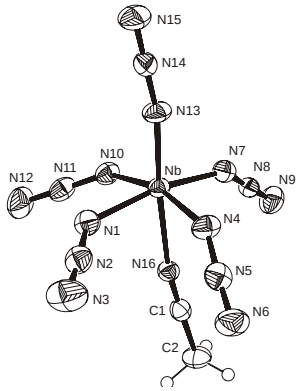

$CH_3CN{\cdot}Nb(N_3)_5$

Supplementary Material

Experimental Evidence for Linear Metal-Azide Bonds. The Binary Group 5 Azides $Nb(N_3)_5$, $Ta(N_3)_5$, $[Nb(N_3)_6]^-$ and $[Ta(N_3)_6]^-$, and 1:1 Adducts of $Nb(N_3)_5$ and $Ta(N_3)_5$ with CH_3CN [**]

Ralf Haiges[*], Jerry A. Boatz, Thorsten Schroer, Muhammed Yousufuddin, and Karl O. Christe[*]

---

[*] Dr. R. Haiges, Dr. T. Schroer, M. Yousufuddin, Prof. Dr. K. O. Christe
Loker Research Institute and Department of Chemistry
University of Southern California
Los Angeles, CA 90089-1661 (USA)
Fax: (+1) 213-740-6679
E-mail: haiges@usc.edu, kchriste@usc.edu
Dr. J. A. Boatz
Space and Missile Propulsion Division
Air Force Research Laboratory (AFRL/PRSP)
10 East Saturn Boulevard, Bldg 8451
Edwards Air Force Base, CA 93524 (USA)

[**] This work was funded by the Air Force Office of Scientific Research and the National Science Foundation. We thank Prof. Dr. G. A. Olah, and Dr. M. Berman, for their steady support, and Prof. Dr. R. Bau and Drs. S. Schneider and R. Wagner for their help and stimulating discussions.

Table S1. Comparison of observed[a] and unscaled calculated vibrational frequencies [cm^{-1}] and intensities[b] for $Nb(N_3)_5$

		observed		calculated (IR)[Raman]	
	description	IR	Ra	B3LYP/SBK+(d)	MP2/SBK+(d)
ν_1	$\nu_{as}N_3$		2155 [10.0]	2235 (62) [1340]	2063 (806) [590]
ν_2	$\nu_{as}N_3$	2124 vs		2209 (2722) [241]	2074 (1918) [141]
ν_3	$\nu_{as}N_3$	2088 vs		2204 (1124) [250]	2061 (1261) [34]
ν_4	$\nu_{as}N_3$		2106 [5.5]	2200 (816) [306]	2059 (391) [246]
ν_5	$\nu_{as}N_3$			2179 (343) [210]	2044 (415) [28]
ν_6	ν_sN_3		1385 [1.6]	1435 (172) [117]	1319 (36) [17]
ν_7	ν_sN_3	1374 m		1403 (611) [31]	1312 (319) [16]
ν_8	ν_sN_3			1375 (252) [8.4]	1294 (122) [20]
ν_9	ν_sN_3	1347 s		1364 (453) [3.9]	1292 (206) [46]
ν_{10}	ν_sN_3			1337 (350) [4.4]	1263 (111) [21]
ν_{11}	δN_3			598 (5.6) [2.8]	596 (5.8) [10]
ν_{12}	δN_3			587 (0.75) [5.8]	575 (83) [2.6]
ν_{13}	δN_3		628 [0.7]	583 (57) [90]	567 (79) [3.4]
ν_{14}	δN_3			580 (48) [2.5]	558 (115) [0.5]
ν_{15}	δN_3		590 sh	580 (51) [0.22]	533 (3.6) [0.39]
ν_{16}	δN_3	591 mw		579 (84) [6.6]	552 (39) [23]
ν_{17}	δN_3			571 (9.7) [77]	521 (4.8) [1.6]
ν_{18}	δN_3	569 w		567 (1.3) [2.1]	519 (6.5) [1.3]
ν_{19}	δN_3			559 (4.2) [0.63]	506 (0.25) [2.3]
ν_{20}	δN_3			552 (2.8) [1.2]	499 (6.4) [3.1]
ν_{21}	$\nu_{as}MN_3$ *eq*	450 sh		472 (164) [5.0]	468 (159) [7.8]
ν_{22}	$\nu_{as}MN_2$ *ax*	440 mw		463 (228) [2.9]	466 (247) [9.6]
ν_{23}	$\nu_{as}MN_2$ *eq*	422 w	427 sh	444 (202) [14]	455 (301) [14]
ν_{24}	ν_sMN_3 *eq*		413 [3.2]	424 (100) [39]	416 (18) [238]
ν_{25}	ν_sMN_2 *ax*		360 sh	363 (0.63) [15]	372 (0.07) [42]
ν_{26}	$\delta_{umbrella}MN_3$		288 [0.7]	285 (9.4) [29]	281 (8.8) [25]
ν_{27}	$\delta_{sciss}MN_3$			266 (1.4) [6.3]	253 (0.37) [11]
ν_{28}	$\delta_{sciss}MN_3$			243 (2.1) [16]	252 (1.2) [31]
ν_{29}	ρMN_2			227 (0.21) [1.2]	212 (0.003) [5.6]
ν_{30}	ρMN_2		234 [0.7]	208 (10) [36]	192 (8.6) [35]
ν_{31}	$\delta_{sciss}MN_2$			143 (0.48) [13]	153 (0.36) [13]
ν_{32}	$\delta_{sciss}MN_2$			134 (0.06) [1.9]	146 (0.11) [4.4]
ν_{33}	τ			103 (0.03) [6.5]	101 (0.11) [4.4]
ν_{34}	τ			100 (0.56) [7.2]	101 (1.9) [19]
ν_{35}	τ			90 (0.13) [0.99]	89 (0.13) [3.7]
ν_{36}	τ			57 (0.34) [15]	68 (0.33) [7.2]
ν_{37}	τ			53 (1.1) [6.3]	48 (1.1) [10]
ν_{38}	τ			45 (0.008) [13]	40 (0.05) [16]
ν_{39}	τ			43 (0.44) [23]	39 (0.17) [29]
ν_{40}	τ			41 (0.25) [20]	32 (0.012) [20]
ν_{41}	τ			29 (0.67) [16]	27 (0.44) [26]
ν_{42}	τ			18 (0.45) [1.7]	6 (0.61) [8.3]

[a] In addition to the bands listed in this table, the following weak infrared bands were observed which are attributed to overtones or combination bands: 1667 w, 1263 w, 1195 sh, 1176 w, 1037 vvw, 696 w, 660 w. [b] Calculated IR and Raman intensities are given in km mol^{-1} and $Å^4$ amu^{-1}.

Table S2. Comparison of observed[a] and unscaled calculated vibrational frequencies [cm^{-1}] and intensities[b] for $Ta(N_3)_5$

		observed		calculated (infrared) [Raman]	
	description	IR	Ra	B3LYP/SBK+(d)	MP2/SBK+(d)
ν_1	$\nu_{as}N_3$		2182 [10.0]	2260 (43) [1109]	2134 (696) [316]
ν_2	$\nu_{as}N_3$	2141 vs		2233 (3271) [125]	2132 (2089) [139]
ν_3	$\nu_{as}N_3$		2129 [3.3]	2217 (895) [259]	2097 (823) [53]
ν_4	$\nu_{as}N_3$	2103 vs		2214 (1202) [170]	2086 (1230) [10]
ν_5	$\nu_{as}N_3$			2210 (319) [246]	2085 (673) [48]
ν_6	ν_sN_3			1473 (7.2) [21]	1348 (29) [88]
ν_7	ν_sN_3	1403 ms		1451 (857) [19]	1334 (368) [6.5]
ν_8	ν_sN_3			1389 (15) [7.9]	1314 (124) [60]
ν_9	ν_sN_3	1364 m		1375 (615) [5.7]	1303 (149) [34]
ν_{10}	ν_sN_3			1370 (450) [10]	1299 (198) [51]
ν_{11}	δN_3			600(2.0) [1.5]	566 (1.6) [0.61]
ν_{12}	δN_3		623 [1.1]	599 (1.2) [15]	562 (0.98) [1.7]
ν_{13}	δN_3	613 mw		586 (13) [0.34]	547 (54) [0.10]
ν_{14}	δN_3			583 (19) [13]	545 (21) [10]
ν_{15}	δN_3		590 sh	576 (2.7) [66]	550 (1.2) [24]
ν_{16}	δN_3			572 (18) [0.59]	543 (0.59) [1.4]
ν_{17}	δN_3			565 (37) [1.7]	538 (1.1) [0.12]
ν_{18}	δN_3	578 w		563 (62) [9.8]	539 (18) [8.2]
ν_{19}	δN_3			560 (9.9) [1.7]	530 (16) [0.08]
ν_{20}	δN_3			552 (4.7) [311]	532 (27) [0.42]
ν_{21}	$\nu_{as}MN_3$ *eq*		450 sh	444 (137) [6.5]	443 (188) [4.0]
ν_{22}	$\nu_{as}MN_2$ *ax*			442 (149) [1.4]	445 (167) [1.7]
ν_{23}	$\nu_{as}MN_2$ *eq*		426 [2.5]	439 (29) [38]	431 (4.3) [172]
ν_{24}	ν_sMN_3 *eq*	410 mw		388 (265) [9.1]	391 (349) [7.1]
ν_{25}	ν_sMN_2 *ax*		390 sh	360 (12) [47]	359 (2.9) [53]
ν_{26}	$\delta_{umbrella}MN_3$			288 (10) [3.2]	282 (11) [4.1]
ν_{27}	$\delta_{sciss}MN_3$			268 (9.8) [10]	255 (20) [5.9]
ν_{28}	$\delta_{sciss}MN_3$		256 [1.7]	258 (5.5) [63]	259 (1.6) [16]
ν_{29}	ρMN_2			253 (3.7) [0.23]	238 (7.5) [0.08]
ν_{30}	ρMN_2		221 [2.0]	207 (22) [21]	189 (22) [4.6]
ν_{31}	$\delta_{sciss}MN_2$			150 (0.18) [5.0]	149 (0.85) [8.9]
ν_{32}	$\delta_{sciss}MN_2$			123 (1.5) [160]	141 (1.5) [11]
ν_{33}	τ			109 (0) [3.6]	115 (0.006) [2.4]
ν_{34}	τ			101 (0.10) [8.4]	94 (0.11) [13]
ν_{35}	τ			100 (0.11) [11]	93 (0.07) [23]
ν_{36}	τ			48 (1.0) [2.6]	42 (0.62) [6.7]
ν_{37}	τ			47 (0.002) [13]	44 (0.07) [11]
ν_{38}	τ			40 (0.36) [47]	35 (0.29) [28]
ν_{39}	τ			40 (0.11) [21]	33 (0.19) [15]
ν_{40}	τ			39 (0.13) [17]	35 (0.005) [24]
ν_{41}	τ			21 (0.65) [0.65]	12 (0.80) [0.73]
ν_{42}	τ			17 (0.70) [3.4]	9 (0.91) [2.2]

[a] In addition to the bands listed in this table, the following weak infrared bands were observed which are attributed to overtones or combination bands: 1669 w, 1508 vw, 1274 sh, 1252 w, 1203 w, 1180 sh, 1036 vw, 850 w, 712 w, 683 w. [b] Calculated IR and Raman intensities are given in km mol^{-1} and $Å^4$ amu^{-1}.

Table S3. Comparison of observed and unscaled calculated[a] vibrational frequencies [cm^{-1}] and intensities for $CH_3CN{\cdot}Nb(N_3)_5$

	description	observed Ra	calculated (infrared) [Raman] B3LYP/SBK+(d)	MP2/SBK+(d)
ν_1	ν_sCH_3	2928 (1.8)	3111 (1.1) [54]	3180 (1.8) [32]
ν_2	$\nu_{as}CH_3$		3110 (1.2) [52]	3179 (1.7) [56]
ν_3	$\nu_{as}CH_3$		3005 (0.82) [192]	3051 (0.83) [173]
ν_4	νCN	2315 (1.2) 2289 (1.1)	2378 (75) [138]	2218 (22) [62]
ν_5	$\nu_{as}N_3$	2140 (10.0)	2238 (751) [1019]	2168 (624) [67]
ν_6	$\nu_{as}N_3$	2121 (1.5)	2202 (1935) [364]	2131 (770) [16]
ν_7	$\nu_{as}N_3$	2097 (1.9)	2176 (1528) [163]	2129 (514) [45]
ν_8	$\nu_{as}N_3$	2090 (1.6)	2176 (1527) [163]	2102 (732) [609]
ν_9	$\nu_{as}N_3$	2074 (2.2) 2058 (1.4)	2153 (0.11) [205]	2100 (1690) [88]
ν_{10}	ν_sN_3		1473 (470) [12]	1460 (17) [8.7]
ν_{11}	$\delta_{sciss}CH_3$	1415 (1.3)	1434 (14) [7.7]	1460 (11) [4.7]
ν_{12}	$\delta_{sciss}CH_3$		1434 (14) [7.6]	1404 (6.6) [8.7]
ν_{13}	ν_sN_3	1351 (1.1)	1413 (246) [4.3]	1345 (252) [35]
ν_{14}	ν_sN_3	1331 (1.1)	1394 (374) [2.2]	1294 (29) [22]
ν_{15}	ν_sN_3		1394 (379) [2.3]	1288 (160) [11]
ν_{16}	ν_sN_3		1391 (6.5) [4.0]	1276 (35) [22]
ν_{17}	δ_sCH_3	1363 (1.2)	1375 (4.9) [16]	1274 (130) [16]
ν_{18}	$\delta_{rock}CH_3$		1046 (0.78)[0.10]	1068 (0.42) [0.67]
ν_{19}	$\delta_{wag}CH_3$		1046 (0.82) [0.10]	1066 (1.4) [0.69]
ν_{20}	νCC	947 (1.0)	934 (8.0) [5.6]	954 (12) [2.7]
ν_{21}	δN_3	620 (1.2)	609 (5.4) [1.7]	612 (14) [15]
ν_{22}	δN_3	610 (1.0)	598 (63) [2.9]	595 (22) [11]
ν_{23}	δN_3		598 (63) [2.9]	594 (111) [8.5]
ν_{24}	δN_3	599 (1.2)	594 (0.61) [0.12]	583 (92) [12]
ν_{25}	δN_3	580 (1.1)	573 (0.006) [0.05]	519 (3.1) [0.31]
ν_{26}	δN_3	566 (1.0)	565 (19) [0.50]	516 (0.46) [0.69]
ν_{27}	δN_3		565 (20) [0.53]	511 (1.5) [4.9]
ν_{28}	δN_3		564 (1.1) [0.03]	509 (6.2) [2.5]
ν_{29}	δN_3	557 (1.1)	557 (12) [1.0]	495 (3.2) [0.88]
ν_{30}	δN_3		557 (12) [1.0]	487 (15) [0.44]
ν_{31}	δN-C-C		456 (21) [0.12]	461 (233) [27]
ν_{32}	δN-C-C		456 (22) [0.12]	454 (261) [1.1]
ν_{33}	νNbN_{ax}	441 (3.1)	444 (224) [31]	451 (272) [17]
ν_{34}	$\nu_{as}NbN_4$	435 (2.8)	427 (278) [1.5]	429 (14) [4.0]
ν_{35}	$\nu_{as}NbN_4$	423 (1.7)	427 (277) [1.5]	428 (20) [81]
ν_{36}	$\nu_{sym}NbN_{4\ i\ p}$	419 (1.7)	411 (0.025) [87]	418 (20) [174]
ν_{37}	$\nu_{sym}NbN_{4\ oo\ p}$	411 (2.0)	352 (0) [3.6]	372 (6.1) [2.9]
ν_{38}	νNbN_{CH3CN}	281 (1.1)	296 (.006) [1.4]	294 (14) [1.5]
ν_{39}	$\delta_{as}NbN_4$	266 (1.3)	278 (17) [0.63]	265 (8.8) [1.2]
ν_{40}	$\delta_{as}NbN_4$	256 (1.3)	278 (17) [0.63]	262 (15) [15]
ν_{41}	δNbN_5	248 (1.4)	255 (0.02) [23]	247 (0.50) [15]
ν_{42}	δNbN_5	226 (1.6)	221 (0.64) [2.1]	232 (1.2) [19]
ν_{43}	δNbN_5		221 (0.66) [2.1]	224 (2.2) [1.7]
ν_{44}	$\delta_{CH3CN-NbN5}$		203 (0.10) [0.34]	202 (4.8) [6.5]
ν_{45}	$\delta_{CH3CN-NbN5}$		203 (0.09) [0.36]	190 (0.01) [2.7]
ν_{46}	δNbN_5	189 (1.3)	200 (0.09) [2.7]	182).96) [12]
ν_{47}	δNbN_5	180 (1.3)	183 (0) [16]	164 (0.01) [4.3]
ν_{48}	τ	139 (1.6)	119 (0.70) [6.6]	117 (0.28) [14]
ν_{49}	τ	96 (2.9)	118 (0.68) [6.6]	115 (1.1)[13]
ν_{50}	τ		83 (0) [0]	64 (2.7) [16]
ν_{51}	τ		52 (3.3) [31]	62 (0.05) [0.81]
ν_{52}	τ		48 (0.004) [24]	59 (0.11) [9.1]
ν_{53}	τ		38 (0.009) [16]	55 (1.7) [31]
ν_{54}	τ		34 (2.1) [1.7]	48 (0.48) [1.9]
ν_{55}	τ		34 (2.0) [1.9]	39 (1.5) [7.3]
ν_{56}	τ		29 (1.6) [3.4]	31 (1.9) [3.7]
ν_{57}	τ		28 (1.7) [3.3]	26 (0.49) [16]

ν_{58}	τ	12 (0.11) [145]	25 (0.89) [16]
ν_{59}	τ	9 (0.11) [15]	20 (0.55) [13]
ν_{60}	unhindered CH_3 τ	13i (0.04) [0.01]	16 (0.008) [19]

[a] Calculated IR and Raman intensities are given in km mol^{-1} and $Å^4$ amu^{-1}, respectively. The given assignments of the observed frequencies are for the calculated B3LYP frequencies. The MP2 values have not been matched with either the B3LYP values or the observed spectrum.

Table S4. Comparison of observed and unscaled calculated[a] vibrational frequencies [cm^{-1}] and intensities for $CH_3CN{\cdot}Ta(N_3)_5$

	description	observed Ra	calculated (infrared) [Raman] B3LYP/SBK+(d)	MP2/SBK+(d)
ν_1	ν_sCH_3		3109 (1.3) [56]	3181 (1.6) [46]
ν_2	$\nu_{as}CH_3$		3109 (1.3) [55]	3179 (2.0) [40]
ν_3	$\nu_{as}CH_3$	2933 [1.7]	3004 (0.96) [202]	3051 (0.71) [166]
ν_4	νCN	2319 [0.5]	2383 (74) [166]	2235 (23) [79]
ν_5	νCN	2291 [0.5]	2222(2045) [360]	2168 (1157) [5.2]
ν_6	$\nu_{as}N_3$	2172 [10.0]	2260 (655) [1025]	2154 (128) [363]
ν_7	$\nu_{as}N_3$	2162 [1.2]	2195 (1739) [125]	2167 (1155) [4.6]
ν_8	$\nu_{as}N_3$	2123 [1.2]	2195 (1735) [125]	2168 (1157) [5.2]
ν_9	$\nu_{as}N_3$	2103 [1.1]	2173 (0.007) [181]	2137 (2378) [92]
ν_{10}	ν_sN_3		1487 (428) [28]	1462 (13) [7.1]
ν_{11}	$\delta_{sciss}CH_3$	1389 [0.4]	1434 (15) [8.2]	1460 (15) [7.1]
ν_{12}	$\delta_{sciss}CH_3$		1433 (15) [8.4]	1404 (4.1) [9.2]
ν_{13}	ν_sN_3		1432 (264) [29]	1364 (260) [69]
ν_{14}	ν_sN_3		1410 (417) [6.8]	1318 (59) [42]
ν_{15}	ν_sN_3		1410 (418) [6.9]	1307 (110) [48]
ν_{16}	ν_sN_3		1409 (0.08)[12]	1301 (181) [27]
ν_{17}	δ_sCH_3	1361 [0.4]	1374 (3.7) [16]	1298 (89) [44]
ν_{18}	$\delta_{rock}CH_3$		1046 (0.91) [0.055]	1067 (0.41) [0.33]
ν_{19}	$\delta_{wag}CH_3$		1046 (0.93) [0.082]	1067 (0.4) [0.33]
ν_{20}	νCC	948 [0.3]	935 (7.5) [15]	958 (12) [3.5]
ν_{21}	δN_3		608 (5.7) [1.2]	592 (2.1) [11]
ν_{22}	δN_3		596 (29) [1.7]	572 (50) [7.1]
ν_{23}	δN_3		596 (28) [1.7]	576 (4.0) [7.3]
ν_{24}	δN_3	592 [0.3]	593 (0.09)) [28]	572 (46)) [6.6]
ν_{25}	δN_3		585 (0.03) [0]	535 (12) [0.37]
ν_{26}	δN_3		584 (1.5) [0.06]	529 (0.10) [0.35]
ν_{27}	δN_3		584 (41) [0.28]	534 (12) [0.30]
ν_{28}	δN_3		584 (43) [0.26]	529 (1.6) [0.06]
ν_{29}	δN_3		578 (0.11) [1.6]	523 (3.8) [0.28]
ν_{30}	δN_3		578 (0.19) [1.6]	523 (2.8) [0.32]
ν_{31}	δN-C-C		471 (1.8) [0.82]	439 (7.1) [0.05]
ν_{32}	δN-C-C		471 (1.9) [0.82]	440 (16) [23]
ν_{33}	νNbN_{ax}	438 [2.1]	424 (0.53) [83]	433 (21) [69]
ν_{34}	$\nu_{as}NbN_4$	417 [0.6]	410 (170) [20]	413 (188) [100]
ν_{35}	$\nu_{as}NbN_4$		398 (242) [0.27]	411 (268) [3.0]
ν_{36}	$\nu_{sym}NbN_{4\ i\ p}$		398 (242) [0.26]	412 (272) [0.67]
ν_{37}	$\nu_{sym}NbN_{4\ oo\ p}$		366 (0) [1.3]	382 (0.32) [3.1]
ν_{38}	νNbN_{CH3CN}		303 (0) [2.1]	297 (0.06) [0.37]
ν_{39}	$\delta_{as}NbN_4$		274 (33) [0.32]	253 (38) [2.0]
ν_{40}	$\delta_{as}NbN_4$		273 (32) [0.31]	253 (40) [1.9]
ν_{41}	δNbN_5	250 [0.7]	246 (3.5) [24]	236 (0.87) [0.83]
ν_{42}	δNbN_5	226 [0.6]	226 (0.43) [0.98]	228 (1.8) [30]
ν_{43}	δNbN_5		226 (0.43) [0.98]	215 (11) [1.2]
ν_{44}	$\delta_{CH3CN-NbN5}$		210 (0.32) [0.12]	215 (10) [1.4]
ν_{45}	$\delta_{CH3CN-NbN5}$		210 (0.32) [0.11]	183 (0.96) [0.79]
ν_{46}	δNbN_5		203 (1.2) [0.27]	182 (0.97) [0.83]
ν_{47}	δNbN_5	192 [0.9]	182 (0.0004) [15]	169 (0) [14]
ν_{48}	τ		126 (0) [0]	107 (2.6) [11]
ν_{49}	τ		115 (0.95) [6.0]	107 (2.4) [11]
ν_{50}	τ		115 (0.96) [6.0]	86 (0.005) [0.006]
ν_{51}	τ		57 (0.0004) [24]	45 (0.027) [24]
ν_{52}	τ		48 (3.7) [28]	42 (4.1) [33]
ν_{53}	τ		40 (2.0) [0.12]	34 (1.1) [2.2]
ν_{54}	τ		40 (2.1) [0.13]	37 (1.2) [2.6]
ν_{55}	τ		33 (1.0) [6.7]	30 (0.0025) [11]
ν_{56}	τ		33 (0.99) [6.7]	17 (0.78) [17]
ν_{57}	τ		30 (0.003) [15]	27 (0.019) [12]
ν_{58}	τ		26 (0.82) [11]	17 (0.34) [16]

ν_{59}	τ	26 (0.77) [11]	15 (0.40) [0.72]
ν_{60}	τ	10 (0.0004) [0.019]	7 (0.66) [0.44]

[a] Calculated IR and Raman intensities are given in km mol^{-1} and $Å^4$ amu^{-1}, respectively. The given assignments of the observed frequencies are for the calculated B3LYP frequencies. The MP2 values have not been matched with either the B3LYP values or the observed spectrum.

Table S5. Comparison of observed and unscaled calculated vibrational frequencies [cm^{-1}] and intensities for $[Ta(N_3)_6]^{-}$[a] in point group C_1

		observed		Calculated (IR) [Raman]	
	description	IR	Ra	B3LYP/SBK+(d)	MP2/SBK+(d)
ν_1	$\nu_{as}N_3$		2159 [10.0]	2238 (100) [940]	2281 (1924) [5.1]
ν_2	$\nu_{as}N_3$	2124 vs	2111 [1.0]	2199 (2670) [120]	2181 (1926) [5.1]
ν_3	$\nu_{as}N_3$	2113 vs	2103 [1.0]	2193 (2307) [130]	2168 (534) [0.86]
ν_4	$\nu_{as}N_3$	2096 vs	2091 [0.8]	2189 (3036) [38]	2169 (771) [0.59]
ν_5	$\nu_{as}N_3$	2087 vs	2081 [0.7]	2178 (8.1) [221]	2169 (59) [1.5]
ν_6	$\nu_{as}N_3$			2172 (176) [193]	2167 (0.021) [444]
ν_7	ν_sN_3			1441 (14) [55]	1304 (0.0004) [123]
ν_8	ν_sN_3	1383 m		1421 (197) [25]	1297 (7.1) [103]
ν_9	ν_sN_3	1372 m		1417 (118) [28]	1298 (6.9) [103]
ν_{10}	ν_sN_3	1360 ms	1355 [0.8]	1414 (336) [18]	1293 (157) [0.003]
ν_{11}	ν_sN_3	1348 s		1412 (420) [7.7]	1292 (232) [67]
ν_{12}	ν_sN_3			1409 (338) [13]	1292 (232) [67]
ν_{13}	δN_3	648 vw		605 (7.4) [0.49]	581 (0.0004) [8.6]
ν_{14}	δN_3	615 m	609 [0.6]	599 (30) [1.2]	563 (13) [4.7]
ν_{15}	δN_3	600 mw		597 (25) [1.6]	563 (12) [4.7]
ν_{16}	δN_3			595 (15) [1.9]	553 (23) [8.0]
ν_{17}	δN_3			594 (0.45) [0.60]	553 (23) [8.0]
ν_{18}	δN_3			592 (10) [0.54]	551 (20) [0.014]
ν_{19}	δN_3			590 (12) [1.4]	534 (0.04) [0.027]
ν_{20}	δN_3			586 (3.4) [0.35]	535 (0) [2.6]
ν_{21}	δN_3	585 mw		585 (16) [0.39]	534 (0.04) [0.029]
ν_{22}	δN_3			584 (20) [0.44]	530 (0.060) [1.1]
ν_{23}	δN_3		582 [0.4]	583 (16) [1.9]	530 (0.063) [1.1]
ν_{24}	δN_3	576 w		578 (17) [0.24]	521 (23) [0]
ν_{25}	νMN	433 w	437 [2.8]	418 (1.9) [73]	414 (0.0009) [155]
ν_{26}	νMN	418 mw		377 (281) [1.3]	389 (294) [0.10]
ν_{27}	νMN	414 mw	372 [0.7]	375 (288) [1.3]	389 (294) [0.10]
ν_{28}	νMN		364 [0.8]	369 (306) [0.63]	369 (357) [0]
ν_{29}	νMN		353 [0.8]	344 (7.4) [1.5]	341 (40) [5.2]
ν_{30}	νMN			337 (41) [2.1]	341 (40) [5.1]
ν_{31}	δMN			271 (31) [3.2]	266 (57) [4.8]
ν_{32}	δMN			261 (31) [2.7]	266 (57) [4.8]
ν_{33}	δMN			254 (9.6) [6.3]	256 (0) [27]
ν_{34}	δMN		225 [1.8]	233 (24) [13]	215 (4.5) [4.7]
ν_{35}	δMN			228 (17) [11]	215 (4.5) [4.7]
ν_{36}	δMN		215 [1.8]	221 (9.6) [7.4]	209 (40) [0]
ν_{37}	δMN		168 [2.6]	181 (0.76) [18]	167 (0) [19]
ν_{38}	δMN			176 (0.06) [7.5]	161 (0.28) [19]
ν_{39}	δMN		160 [2.6]	172 (0.34) [14]	161 (0.28) [19]
ν_{40}	τ			91 (0.55) [7.3]	79 (3.6) [0]
ν_{41}	τ			83 (0.13) [10]	44 (0.006) [19]
ν_{42}	τ			79 (0.48) [0.69]	44 (0.004) [19]
ν_{43}	τ			44 (2.4) [19]	43 (0) [28]
ν_{44}	τ			41 (0.81) [18]	37 (1.7) [16]
ν_{45}	τ			39 (1.2) [18]	37 (1.8) [16]
ν_{46}	τ			38 (0.47) [17]	28 (0.73) [28]
ν_{47}	τ			36 (2.8) [11]	28 (0.75) [28]
ν_{48}	τ			35 (1.4) [7.3]	27 (0.0004) [3.6]
ν_{49}	τ			30 (0.44) [3.9]	14 (0.60) [6.5]
ν_{50}	τ			27 (0.22) [10]	14 (0.58) [6.3]
ν_{51}	τ			22 (0.81) [6.5]	9 (2.8) [0.002]

[a] Calculated IR and Raman intensities are given in km mol^{-1} and $Å^4$ amu^{-1}, respectively; observed spectra are for the solid $[P(C_6H_5)_4]^+$ salt. The MP2 values have not been matched with either the B3LYP values or the observed spectrum.